The FASEB Journal

FASEB
Federation of American Societies for Experimental Biology

RESEARCH ARTICLE OPEN ACCESS

Effects of Cannabidiol on *TAFAZZIN*-Deficient B-Lymphoblastoid Cells

John Z. Chan | Antonia N. Berdeklis | Ming Rong Liu | Fasih A. Rahman | Michelle V. Tomczewski | Mackenzie Q. Graham | Musa Musa | Alex D. Cocco | Ken D. Stark | Joe Quadrilatero | Robin E. Duncan

Department of Kinesiology and Health Sciences, Faculty of Health, University of Waterloo, Waterloo, Ontario, Canada

Correspondence: Robin E. Duncan (reduncan@uwaterloo.ca)

Received: 16 September 2025 | **Revised:** 5 January 2026 | **Accepted:** 27 February 2026

Keywords: Barth syndrome | B-lymphoblastoid cells | Cannabidiol | Cardiolipin | electron transport chain | mitochondria | TAFAZZIN

ABSTRACT

Barth Syndrome (BTHS) is a debilitating X-linked genetic disorder caused by mutations in the gene encoding TAFAZZIN, an enzyme responsible for the remodeling of cardiolipin. While cyclic neutropenia is a well-recognized immunological feature of this disease, emerging evidence suggests that lymphopenia may also occur. The objective of this study was to examine the effects of cannabidiol (CBD) on growth, cardiolipin content, and mitochondrial abnormalities in BTHS patient-derived B-lymphoblastoid cells. CBD (1 μM) restored the growth of BTHS B-lymphoblastoids to healthy control levels, but did not alter cell cycle distribution or sub-G1 cell populations, which surprisingly also did not differ from healthy control B-lymphoblastoids. CBD treatment also fully restored the total cellular cardiolipin concentration and reversed the elevation in monolysocardiolipin/cardiolipin ratio in BTHS B-lymphoblastoids to healthy cell levels, but did not restore the cardiolipin fatty acyl composition. Assessment of mitochondrial markers suggested that increased cardiolipin did not result from increased mitochondrial content. This improvement in cardiolipin concentration was associated with a significant increase in the maximal coupled state III respiration of BTHS B-lymphoblastoids, with all five tested BTHS donors exhibiting increased mitochondrial membrane potential following CBD treatment. CBD fully reversed the deficit in succinate dehydrogenase subunit A in BTHS cells, and partially reversed deficits in cytochrome c oxidase subunits I and IV, and partially restored supercomplex I/III_2 levels, but did not rescue I/III_2/IV levels. This work suggested a potential role for CBD as a therapeutic in BTHS B-lymphopenia that merits further investigation.

1 | Introduction

Barth Syndrome (BTHS) is an ultra-rare X-linked recessive disorder that affects approximately 1 in every 300 000 to 400 000 live births, with only 230–250 cases reported worldwide [1, 2]. The disease appears to have arisen spontaneously multiple times, with more than 200 reported unique mutations within the *TAFAZZIN* gene identified among the clinical population, encoding for dysfunctional TAFAZZIN proteins [3]. Loss of enzyme activity of TAFAZZIN results in the impaired fatty acyl side chain remodeling of newly synthesized nascent cardiolipin into the mature and tissue-specific form that is needed to maintain proper cellular function [4–6]. As a consequence, *TAFAZZIN*-deficient cells and tissues have reduced endogenous cardiolipin levels [7, 8], and much has been learned about the role of this specialized lipid from their study. For example, decreases in cardiolipin content in TAFAZZIN-deficient cells and tissues are linked to mitochondrial dysfunction caused by abnormal cristae alignment, decreased electron transport chain (ETC) capacity, and dysregulated mitochondrial dynamics [4, 9–12].

Tissues and cells with higher energetic demands are often more affected in BTHS, including the heart, the skeletal muscle, and the immune system [13–15]. While research on immune dysfunction

Ming Rong Liu and Fasih A. Rahman contributed equally to this work.

in BTHS has primarily focused on the etiology and treatment of neutropenia as a prominent clinical feature of the syndrome [16–20], more recent studies have suggested that generalized impairments in the adaptive immune system are also common [21, 22]. For example, Corrado et al. (2020) analyzed the peripheral blood mononuclear cells (PBMCs) from adolescent BTHS patients and found lower levels of CD8+ T lymphocytes, as well as a lower percentage of CD8+ cells producing interferon-γ, a pro-inflammatory cytokine critical for induction and modulation of both innate and adaptive immune responses [21]. Additionally, in a case report by Kudlaty et al. (2022), a 2-month-old male BTHS patient experiencing repeated bouts of bacterial and viral infections was found to have both persistent neutropenia and B cell lymphopenia, with resultant hypogammaglobulinemia [23]. Impaired adaptive immune function in *TAFAZZIN* deficiency therefore warrants more detailed investigation.

In light of this, previous work from our group has identified a reduction in the growth of B-lymphoblastoid cell populations derived from patients with BTHS when compared to those derived from healthy sex- and age-matched control donors [11]. In that report, the treatment effects of an endocannabinoid-like compound, oleoylethanolamide (OEA), were also investigated, and a beneficial effect on cell growth was observed, with approximately half of the gap in cell numbers being closed after 4 days of culture [11]. Additional study demonstrated that OEA significantly reversed impairments in mitochondrial dynamics and reduced the percentage of abnormally large mitochondria, indicating functionally relevant benefits [11]. However, while promising, OEA treatment did not significantly improve the content or composition of cardiolipin [11]. Furthermore, OEA also reportedly possesses anorexigenic properties when used as a nutraceutical, which could limit its utility in the clinical BTHS population where gastrointestinal symptoms are common [11, 24]. Thus, we changed our focus to the investigation of alternative related compounds that could provide a more favorable safety profile and potentially a more complete rescue of cellular and mitochondrial parameters.

In the current work, we investigate effects of cannabidiol (CBD) on BTHS B-lymphoblastoid cells. CBD, a phytocannabinoid derived from the *Cannabis sativa* plant, was first isolated from a strain of hemp in the 1940s [25, 26]. More recently, it has emerged as a promising therapeutic compound with a wide range of biological effects, including an ability to influence numerous mitochondrial functions (e.g., calcium homeostasis, apoptosis, ETC activity, biogenesis, network dynamics, etc.) [27]. Due to the central role of mitochondria in energy production and cellular health, dysfunction associated with this organelle has been implicated in a wide variety of diseases including neurodegenerative disorders, cardiovascular conditions, diabetes, and several cancers [27–29]. A greater understanding of the impact of CBD on mitochondrial function is therefore relevant to many conditions, in addition to BTHS, as well as to normal health.

2 | Materials and Methods

2.1 | Materials

High purity CBD (Product #ISO60156, certified reference material, analytical purity >98.5%) was obtained from Cayman Chemical Company (Ann Arbor, MI, USA). Epstein–Barr virus transformed B-lymphoblastoid cells derived from five male subjects with BTHS and five age- and sex-matched apparently healthy individuals were obtained from the Coriell Institute for Medical Research (Camden, NJ, USA) under a material transfer agreement with the University of Waterloo. Specific patient characteristics can be found in Table 1. Ethical approval for the use of these cells was received from the University of Waterloo Research Ethics Board (Protocol #40551). Unless otherwise stated, all other reagents were from Thermo Fisher Scientific (Waltham, MA, USA).

2.2 | Cell Culture

Cells were routinely subcultured in suspension in T25 vented-cap flasks, in Roswell Park Memorial Institute (RPMI) medium (Wisent Bioproducts, Saint-John Baptiste, QC, Canada) supplemented with 10% fetal bovine serum (Gibco, Waltham, MA, USA) with 1% penicillin–streptomycin (Gibco, Waltham, MA, USA) at 37°C in a 5% CO_2 environment. For all experiments, cells were initially seeded at a density of 1.2×10^6 cells per flask in RPMI with 10% charcoal-stripped fetal bovine serum and 1% penicillin–streptomycin and then treated with 1 μM concentrations of CBD (Cayman Chemical, Ann Arbor, MI; ≥98% purity) or vehicle alone (0.1% ethanol final concentration) for the number of days indicated. Pharmacokinetic studies indicate that dosing in humans results in blood concentrations that range from the nanomolar range to 2–3 μM [27], and therefore a 1 μM concentration was chosen based on pharmacological relevance.

2.3 | Cell Growth

For the assessment of total cell numbers, cells were first gently mixed in suspension by pipetting with a 10 mL pipette, and then samples were manually counted using a hemacytometer. Counting was conducted every 24 h starting from day zero, over a period of 4 days [11].

TABLE 1 | Characteristics of individual BTHS and healthy donors.

Cell line ID	Sex	Age (years)	Mutation type
GM22192	Male	10	Missense (p.R94C)
GM22163	Male	9	Frameshift (p.Gly58AlafsX25)
GM22193	Male	10	Nonsense (p.L166X)
GM22150	Male	7	Nonsense (p.W79X)
GM22194	Male	9	Deletion of G4.5
AG15022	Male	10	Apparently healthy
AG14731	Male	8	Apparently healthy
AG14948	Male	10	Apparently healthy
AG14750	Male	9	Apparently healthy
AG14947	Male	10	Apparently healthy

2.4 | Flow Cytometry

Flow cytometry experiments were performed as previously described [30]. After 2 days of treatment, BTHS and healthy B-lymphoblastoids were washed three times with phosphate buffered saline (PBS) and then fixed in 1 mL of ice-cold 70% ethanol and stored at 4°C for 24 h. For cell cycle analysis, fixed cells were then pelleted, washed twice more with PBS, and incubated with RNase A (20 μg/mL) and propidium iodide (50 μg/mL) for 30 min at room temperature. Propidium iodide was excited with a 488 nm laser and fluorescence was collected in the FL2 channel (585/42 nm bandpass filter). Events were gated on forward scatter vs. side scatter to exclude debris and DNA-content histograms of FL2-H (linear scale) were analyzed to determine sub-G1, G1, S, and G2/M phase distributions, expressed as a percentage of gated events.

For mitochondrial membrane potential measurements, live cells were incubated with 50 nM tetramethylrhodamine ethyl ester (TMRE; Sigma, Cat# 87917) in PBS containing 1 g/mL glucose at 37°C for 30 min in the dark. Prior to acquisition, cells were gently resuspended to ensure a uniform single-cell suspension. Events were gated on forward scatter vs. side scatter to exclude debris and the gated lymphoblast population was used directly for analysis as cells remained in a uniform suspension with minimal aggregation. TMRE signal intensity was quantified as the mean fluorescence intensity of gated cells (FL2 channel; 585/42 nm bandpass filter), reflecting relative mitochondrial membrane potential. Flow cytometry was performed on a FACSCalibur system (BD Biosciences), and data were analyzed using CellQuest Pro software (BD Biosciences).

2.5 | Mitochondrial Respirometry

Oxygen consumption measurements were conducted using the O2K-FluoRespirometer (Oroboros Instruments). After 4 days of treatment, BTHS and healthy B-lymphoblastoids were counted using a hemacytometer, and approximately two million cells were transferred to a respirometry chamber containing 2 mL of respiration buffer (105 mM K-MES, 1 mM EGTA, 5 mM $MgCl_2$, 30 mM KCl, 10 mM KH_2PO_4, and 5 mg/mL BSA; pH 7.1), supplemented with 10 μM Amplex Red, 5 U/mL horseradish peroxidase, and 0.5 U/mL superoxide dismutase. To permeabilize the cells, digitonin (25 μg/mL final concentration) was introduced at the outset of the experiment.

Measures of oxygen consumption started with the sequential addition of mitochondrial substrates, including pyruvate (5 mM), malate (0.5 mM), and glutamate (10 mM) to examine Complex I (CI)-mediated leak respiration (State 2—Complex I). Next, succinate (10 mM) was added to evaluate Complex II (CII) leak respiration (State 2—Complex I + II), followed by ADP (2500 μM) to induce maximal coupled respiration (State 3). Finally, Cytochrome C (Cyt c) (10 μM) was introduced into the chamber to assess mitochondrial outer membrane integrity. All procedures were completed within 1 h to preserve cell viability.

2.6 | Thin Layer Chromatography—Gas Chromatography

The isolation and analysis of cardiolipin was performed essentially as we have previously described [11]. Following 4 days of CBD treatment, BTHS and healthy B-lymphoblastoids were pelleted, washed three times with PBS, and homogenized in 1 mL of PBS using a TissueLyser II for 2 min at a frequency of 25 Hz. Total lipids were extracted from the homogenized sample using a 3.75 mL chloroform and methanol mixture (1:2, v:v) [31]. Subsequently, 1.25 mL of chloroform and 1.25 mL of ddH_2O were added to the sample, vortexed, and centrifuged at 1734 *g* for 5 min. The lower organic phase was carefully collected and dried under a stream of nitrogen gas.

To isolate individual phospholipid species, the organic phase was reconstituted in chloroform and applied to a Silica Gel HF plate measuring 20 × 20 cm with a layer thickness of 250 μm (Analtech Inc., Cole-Parmer Canada, Montreal, QC, Canada), and resolved by thin-layer chromatography using a solvent system containing chloroform:methanol:2-propanol:0.25% KCl:trimethylamine (30:9:25:6:18, v/v/v/v/v), also as previously described [32]. Phospholipid bands were visualized using UV illumination after a spray with 0.1% 2,7-dichlorofluorescein in methanol, and identified by comparison with known standards (Avanti Polar Lipids, Millipore Sigma, Mississauga, ON, Canada). The bands corresponding to cardiolipin and monolysocardiolipin (MLCL) were scraped for gas chromatography (GC) analysis.

Fatty acids within cardiolipin and MLCL were esterified to fatty acid methyl esters on a heating block for 1 h at 95°C using 14% boron trifluoride in methanol and hexane, with nonadecanoic acid (19:0) as an internal standard (Nu-Chek Prep, Elysian, MN, USA) [33]. After esterification, each of the samples was centrifuged at 3000 rpm for 5 min, and the hexane layer was extracted into a new glass tube and dried under nitrogen gas, followed by a subsequent reconstitution in heptane. GC with flame ionization detection (Scion Instruments Canada, Edmonton, AB, Canada) was performed as described in detail previously [34]. In brief, the gas chromatograph was equipped with a DB-FFAP (15 m length × 0.10 mm inner diameter × 0.10 μm film thickness) nitroterephthalic acid-modified polyethylene glycol capillary column (J&W Scientific/Agilent Technologies, Mississauga, ON, Canada) with hydrogen as the carrier gas and temperature ramping to optimize resolution of each fatty acid.

The fatty acid composition data was expressed both as relative mass percentages, representing the proportionate mass of each fatty acid within the total mass of fatty acids analyzed, and as concentrations showing the mass of fatty acids in the cardiolipin fraction normalized per mg of protein in cell pellets. Total cardiolipin fatty acid mass normalized to cell protein was used as a proxy for the total amount of cardiolipin in a sample.

2.7 | Reverse Transcription-Quantitative Polymerase Chain Reaction (RT-qPCR)

Following 4 days of treatment, the cells were harvested, and RNA was extracted using TRIzol Reagent (Invitrogen, Carlsbad,

CA) as we have previously described [32]. Next, a High-Capacity complementary DNA (cDNA) Reverse Transcription Kit was used to reverse transcribe the RNA samples into cDNA, essentially as described in the manufacturer's instructions (Applied Biosystems, Waltham, MA, USA). Briefly, 2 μg RNA in 10 μL ddH_2O was added to 10 μL of a reverse-transcription master mix containing 2 μL of 10× RT buffer, 0.8 μL of dNTP mix (100 nM), 2 μL of random hexamer primers, 1 μL of Reverse Transcriptase, and 4.2 μL of ddH_2O in a thin-walled 96-well plate, and incubated in a T100 Thermocycler (Bio-Rad, Hercules, CA) under the following conditions: 25°C for 12 min, 37°C for 120 min, and 85°C for 5 min, followed by a hold at 4°C until storage at −20°C.

For quantitative polymerase chain reaction (qPCR) assays, 1 μL of cDNA was added to a 96-well thin-walled plate containing 5 μL PerfeCTa SYBR Green (QuantaBio, Beverly, MA, USA) master mix, 1 μL each of forward and reverse primers (25 μM in ddH_2O), and 3 μL of ddH_2O. Primer sequences used in qPCR analyses are listed in Table S1. Samples were run in the CFX-96 Connect Real-Time PCR Detection System (BioRad, Hercules, CA) with cycling conditions set at 95°C for 2 min, followed by 49 cycles of 95°C for 10 s and 60°C for 20 s. Relative gene expression levels were calculated using the ΔΔCt method, with the Ct values normalized to *glyceraldehyde-3-phosphate dehydrogenase* (*GAPDH*) as a loading control.

2.8 | Imaging Flow Cytometry

Analysis of mitochondrial mass was determined using flow cytometry as described previously [35, 36]. Cells were pelleted by centrifugation at 300 *g* for 5 min, and the resulting pellets were resuspended in 200 μL of PBS containing 50 nM MitoTracker Green FM Dye and 1 mg/mL glucose. Cell samples were gently agitated and incubated for 30 min at 37°C. Subsequently, cell samples were centrifuged and resuspended in PBS containing 1 mg/mL glucose and were stored at 37°C until analysis.

Cell images were acquired at 60× magnification using an ImagestreamX MK II cytometer (Cytek Biosciences, Fremont, CA) equipped with 488 and 785 nm excitation lasers, which were set to 30 and 188 W, respectively. Channels-1, −2 and −5 were set to brightfield illumination, green filter, and side scatter, respectively. Analysis was conducted using the IDEAS 6.2 software. Sample gating was based on (1) intermediate area against high aspect ratio to select for single cells, (2) high gradient root mean squared to select for focused cells, (3) a median raw centroid × value to select for cells centered in the image, and (4) MitoTracker emission intensity against area to select for stained cells. This selected pool of cells was analyzed for cellular area using the area function on the brightfield channel (Ch01), and spot area using the spot area function on the green emission channel (Ch02). The mean spot area was normalized to the mean cellular area to determine the mean percentage mitochondrial area.

2.9 | Immunoblotting

Western blotting analysis was performed as previously described, with minor modifications [37]. Cells were collected on day four into 50 mL Falcon tubes and centrifuged at 1000 *g* for 5 min. The supernatant was removed, and samples were washed three times with PBS. After the final wash, protein lysates were prepared by suspending the cell pellet in RIPA buffer (50 mM Tris–HCl, pH 8.0; 150 mM NaCl, 1% Nonidet P-40, 0.5% sodium deoxycholate, and 0.1% SDS) supplemented with 10 μL/mL of protease/phosphatase inhibitor cocktail (Cell Signaling, Beverly, MA), and protein concentrations were determined using bicinchoninic acid assay. Samples were mixed with 5 μL of 4× Laemmli Buffer and heated to 95°C for 5 min, followed by electrophoresis through 10% SDS-PAGE TGX Stain-Free FastCast gels (Bio-Rad Canada) at 120 V for 1 h. Transfer onto polyvinylidene fluoride (PVDF) membranes was achieved using a Bio-Rad Trans-Blot Turbo system set at 25 V for 30 min. Subsequently, the membranes were blocked with 5% BSA in Tris-buffered saline with Tween 20 (TBST) for 1 h at room temperature, then incubated overnight at 2°C in TBST containing 5% BSA and primary antibodies (1:1000 dilution) obtained from Cell Signaling Technology (Beverly, MA, USA). After three washes with TBST, the membranes were incubated with TBST containing HRP-conjugated secondary antibodies (1:2000 dilution) and 5% BSA for 1 h at room temperature, followed by three 10 min washes with TBST. Finally, membranes were placed in 1 mL of LumiGLO for 1 min, and bands were detected using a ChemiDOC Touch Imaging System (Bio-Rad Canada). Protein bands were normalized to total loaded protein that was imaged in TGX Stain-Free gels, which cause proteins to fluoresce when placed under UV trans-illumination. Relative protein levels were detected using Image Lab software (Bio-Rad Canada).

2.10 | Blue Native Polyacrylamide Gel Electrophoresis (BN-PAGE)

Mitochondrial isolation was performed as previously described [12]. Briefly, BTHS and healthy B-lymphoblastoids were treated with vehicle or 1 μM CBD for 3 days, then harvested and washed three times with PBS, and resuspended in a 1 mL mitochondrial isolation buffer containing 20 mM 4-(2-Hydroxyethyl)piperazine-1-ethanesulfonic acid (pH 7.6), 220 mM mannitol, 70 mM sucrose, 1 mM EDTA, 1% protease-phosphatase inhibitor cocktail (Cell Signaling), and 2 mg/mL of BSA. To lyse the cells, 30 passes were performed with a drill-fitted pestle in a 2 mL glass homogenizer within a 4°C ice slurry bath, followed by centrifugation at 600 *g* to pellet cell debris and nuclei. The resulting supernatant, containing the mitochondrial fraction, was transferred to a fresh tube and centrifuged at 10000 *g* to pellet the mitochondria. The supernatant was discarded, and the mitochondrial pellet was resuspended in mitochondrial isolation buffer. Total mitochondrial protein content was quantified using a bicinchoninic acid assay.

Mitochondria (equivalent to 50 μg of protein) were pelleted and solubilized in 12 μL of 1 × NativePAGE sample buffer containing digitonin (8 g/g protein), followed by incubation for 20 min at 4°C. Insoluble material was removed by centrifugation at 20000 *g* for 20 min, and the supernatant was combined with 1 μL Coomassie Brilliant Blue G-250 (10% w/v). Next, the anode buffer and the dark/light blue cathode buffers were made according to the manufacturer's protocol using the 10 × NativePAGE Running Buffer and the 20 × NativePAGE Cathode Additive. The samples

were loaded into NativePAGE Novex 3%–12% Bis-Tris Gels, and the upper chamber was filled with the dark blue cathode buffer (containing 0.02% (w/v) Coomassie Brilliant Blue G-250), and the lower chamber with anode buffer. Electrophoresis was performed for approximately 30 min at 100 V until the dye front reached 1/3 of the gel, at which point the dark blue buffer was replaced with light blue cathode buffer (0.002% w/v Coomassie Brilliant Blue G-250). The run was continued for an additional 1.5 h, increasing the voltage by 50 V every 20–30 min at 4°C.

Gels were transferred to PVDF membranes using a Mini Blot Module (Thermo Fisher) at 25 V for 90 min. Membranes were incubated in 8% (v/v) acetic acid for 15 min and reactivated in methanol. Immunodetection was performed using standard western techniques as described above. To quantify the relative supercomplex content between vehicle and CBD treated BTHS and healthy B-lymphoblastoids, 3 μL of the mitochondrial fraction solubilized by digitonin was aliquoted and mixed with 10 μL of ddH_2O and 5 μL of 4× Laemmli Buffer and heated to 95°C for 5 min and run on a 10% SDS-PAGE TGX Stain-Free FastCast gel (Bio-Rad Canada) at 120 V for 1 h. Quantification was performed using Image Lab software (Bio-Rad Canada), and BN-PAGE band intensities were normalized to total protein loading visualized in the Stain-Free gel.

2.11 | Statistical Analyses

Data are expressed as means ± S.E.M. Repeated measures two-way ANOVA with multiple comparisons using Sidak's post hoc test was used to analyze for the effects of treatments within cell types. Effects of cell type within each treatment, and interactions between cell types and treatments were assessed using a two-way analysis of variance (ANOVA) with Sidak's post hoc test. Differences between treated and untreated cells for individuals were assessed by Student's paired *t*-test. Differences were considered significant when $p < 0.05$.

3 | Results

3.1 | Treatment With CBD Fully Rescues a Deficit in BTHS B-Lymphoblastoid Colony Growth

Cells were seeded on day zero at a density of 1.2×10^6 cells/flask (Figure 1A). Significant growth impairment of the *TAFAZZIN*-deficient cells was evident by 72 h, when the BTHS B-lymphoblastoid lines had expanded only to a mean of ~3.0 million cells, while the mean healthy B-lymphoblastoid count was ~4.3 million (Figure 1A, Table S2). Data on vehicle-treated healthy and

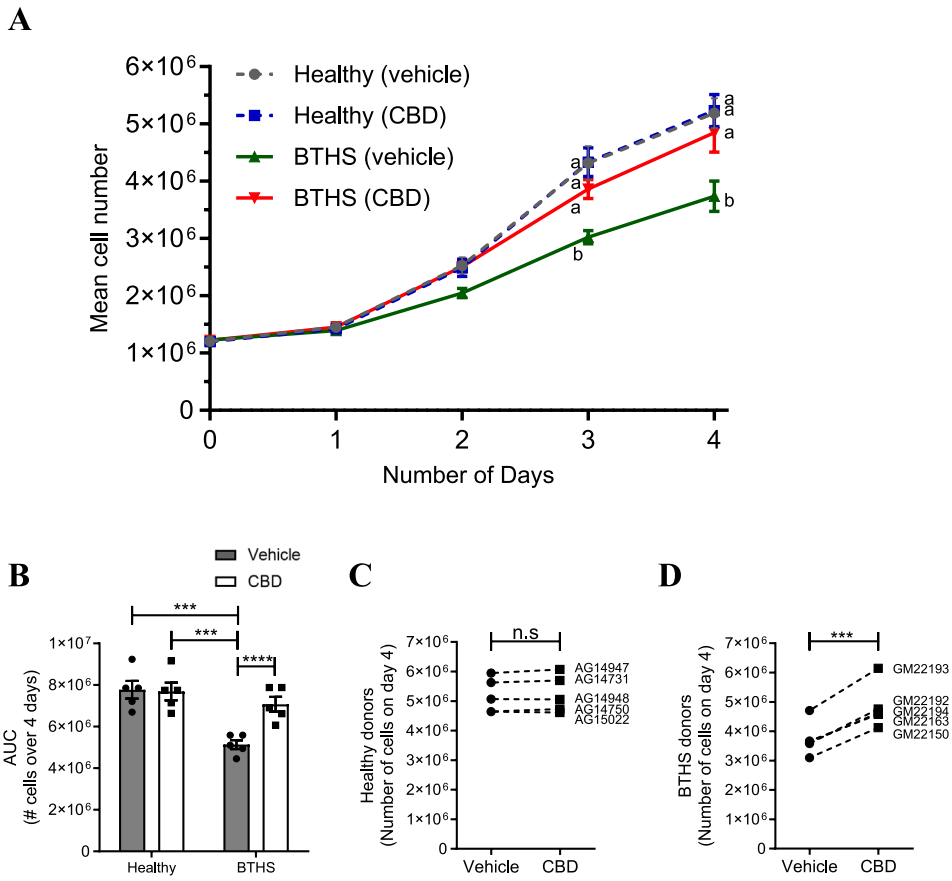

FIGURE 1 | CBD treatment fully reverses the BTHS B-lymphoblastoid growth impairment. Mean cell numbers from cultures of five BTHS and healthy B-lymphoblastoid lines treated for 4 days with either vehicle control (0.1% (v/v) ethanol) or 1 μM CBD are shown (A), with corresponding incremental area-under-the-curve (AUC) analysis (B). The relative response to CBD treatment is depicted as the number of vehicle- or CBD-treated cells on day 4 for each individual healthy (C) or BTHS (D) line. Data are presented as means ± S.E.M; $n = 5$. [ab]Group means with different letters are significantly different when comparisons are made at the same timepoint ($p < 0.05$), ***$p < 0.001$, ****$p < 0.0001$, n.s. = not significantly different.

BTHS B-lymphoblastoids have been reported previously, when all lines were cultured, treated, and counted in experiments also performed with OEA [11]. By 96 h, the gap between mean BTHS and healthy counts had increased, with the BTHS count reaching ~3.7 million cells compared to the ~5.2 million cells in the healthy control group. Treatment with CBD, however, fully rescued this deficit in growth by increasing the mean number of BTHS cells to ~3.9 million at 72 h and ~4.8 million at 96 h, which did not differ significantly from healthy lines at either timepoint. Notably, CBD had no significant effect on the growth of healthy lines (Figure 1A,B). Determination of the mean growth patterns through assessment of incremental area-under-the-curve similarly illustrates the striking nature of the overall rescue (Figure 1B).

Each lymphoblastoid line originates from a unique donor with inherent differences in characteristics. For example, despite equal seeding at day zero, total cell counts by day four varied by up to 1.3×10^6 cells among healthy lines, and as much as 2.0×10^6 cells among BTHS B-lymphoblastoid lines. Thus, we graphed the total cell number on day four in vehicle-only versus CBD-treated lines and performed a pair-wise comparison, in order to better capture the occurrence of clinically meaningful effects. While CBD had no measurable impact on the number of healthy cells in culture on day four (Figure 1C), all five individual BTHS lines demonstrated a positive response to CBD treatment compared to vehicle alone, indicating therapeutic reversal of a growth deficit that is unique to the BTHS lines (Figure 1D).

3.2 | Cell Cycle Phase Proportions of BTHS and Healthy B-Lymphoblastoids Are Similar on Day 2 and Not Significantly Altered by CBD

Cell number differences can result from alterations in the gain of cells (i.e., proliferation) or loss of cells (i.e., death) over time. The cell cycle phase distribution of B-lymphoblastoids was assessed on day 2 of growth, 1 day prior to the emergence of statistically significant differences in cell numbers. The subG1 population describes cells with fragmented DNA, which is highly characteristic of apoptosis, although it may also be detected to a lesser extent in other forms of cell death [38]. Surprisingly, there was no significant difference on day 2 in subG1 events between BTHS and healthy B-lymphoblastoids treated with vehicle only (Figure 2A,B, Table S3). In addition, CBD treatment did not significantly change the subG1 population in either BTHS or healthy cells (Figure 2A,B, Table S3). The G1 phase denotes cells that are growing and in preparation for DNA synthesis [39]. Our analysis showed that the proportion of cells within the G1 phase was not significantly different between BTHS and healthy B-lymphoblastoids under either vehicle- or CBD-treated conditions (Figure 2A,B, Table S3). Further analysis of the proportion of cells in S and G2/M phases, which encompass DNA synthesis and mitosis [39], respectively, also showed no significant differences between BTHS and healthy cells, and no effect of treatment (Figure 2A,B, Table S3).

3.3 | CBD Restores Cardiolipin Concentration and the MLCL/CL Ratio in BTHS B-Lymphoblastoids

The effects of 1 μM CBD on total cardiolipin concentration, measured as micrograms of cardiolipin fatty acyls per mg of protein in a sample, were examined in both healthy and BTHS B-lymphoblastoids (Figure 3A, Table S4). As expected, vehicle-treated BTHS B-lymphoblastoids had a significantly lower cardiolipin concentration compared to vehicle-treated healthy cells (3.31 ± 0.32 μg cardiolipin fatty acyls/mg protein versus 5.72 ± 0.39 μg cardiolipin fatty acyls/mg protein, respectively, $p = 0.0144$). This resulted primarily from a ~2/3 lower level of cellular cardiolipin monounsaturated fatty acyl (MUFA) content and an ~3/4 lower level of cellular cardiolipin N-6 polyunsaturated fatty acyl (PUFA) content in vehicle-treated BTHS B-lymphoblastoids compared to vehicle-healthy control cells, while cellular cardiolipin saturated fatty acyl (SFA) and N-3 PUFA cardiolipin concentrations did not differ significantly (Figure 3B).

CBD treatment dramatically restored the cardiolipin concentration in BTHS B-lymphoblastoids to 5.60 ± 0.51 μg cardiolipin fatty acyls/mg of cell protein, essentially matching healthy cell levels and producing a dramatic full rescue of this lipid deficiency. Interestingly, however, this effect did not result from a reversal of the loss of cellular concentrations of cardiolipin containing monounsaturated (MUFA) and N-6 polyunsaturated fatty acyls (PUFA), but rather from an increase by more than 50% in the cellular concentrations of cardiolipin containing SFA and N-3 PUFA (Figure 3B).

In healthy cells, CBD treatment did not significantly alter the total cardiolipin concentration (Figure 3A) or the concentrations of cardiolipin when grouped by content of major fatty acyl types (Figure 3B), indicating that changes were specific to BTHS B-lymphoblastoid cells. Notably, changes in cardiolipin concentration helped to restore the monolysocardiolipin/cardiolipin (MLCL/CL) ratio in CBD-treated BTHS B-lymphoblastoids to healthy cell levels, also without altering ratios in healthy cells (Figure 3C).

To further assess the effects of CBD on cardiolipin composition, the relative proportions of individual fatty acyls within cardiolipin were expressed as a percentage of the total mass of cardiolipin analyzed (wt/wt%) (Figure 3D–G). Under vehicle-treated conditions, BTHS B-lymphoblastoids had a higher relative abundance of SFAs within cardiolipin than healthy B-lymphoblastoids, and this was primarily driven by a higher proportion of palmitate (16:0) and a minor but measurably higher level of laurate (12:0) (Figure 3D). In contrast, MUFAs were ~1/3 less abundant in cardiolipin from BTHS B-lymphoblastoids compared to healthy cells, and this was driven by significantly lower relative percentages of palmitoleic acid (16:1n-7) and oleic acid (18:1n-9) (Figure 3E). The relative abundance of N-6 PUFAs within cardiolipin was also lower in vehicle-treated BTHS B-lymphoblastoids compared to healthy cells by 60.5%, primarily due to lower levels of linoleate (18:2n-6) and dihomo-gamma-linolenate (20:3n-6) (Figure 3F). There was no significant difference in the relative abundance of total N-3 PUFAs between vehicle-treated BTHS and healthy B-lymphoblastoids, although the relative proportion of alpha-linolenic acid (18:3n3) was higher in vehicle-treated BTHS compared to healthy B-lymphoblastoids (Figure 3G).

Surprisingly, although CBD increased the total concentration of cardiolipin in treated relative to vehicle-only BTHS B-lymphoblastoids (Figure 3A), as well as the concentrations of cardiolipin containing SFAs and N-3 PUFAs in these cells (Figure 3B), it did not significantly alter the relative proportions

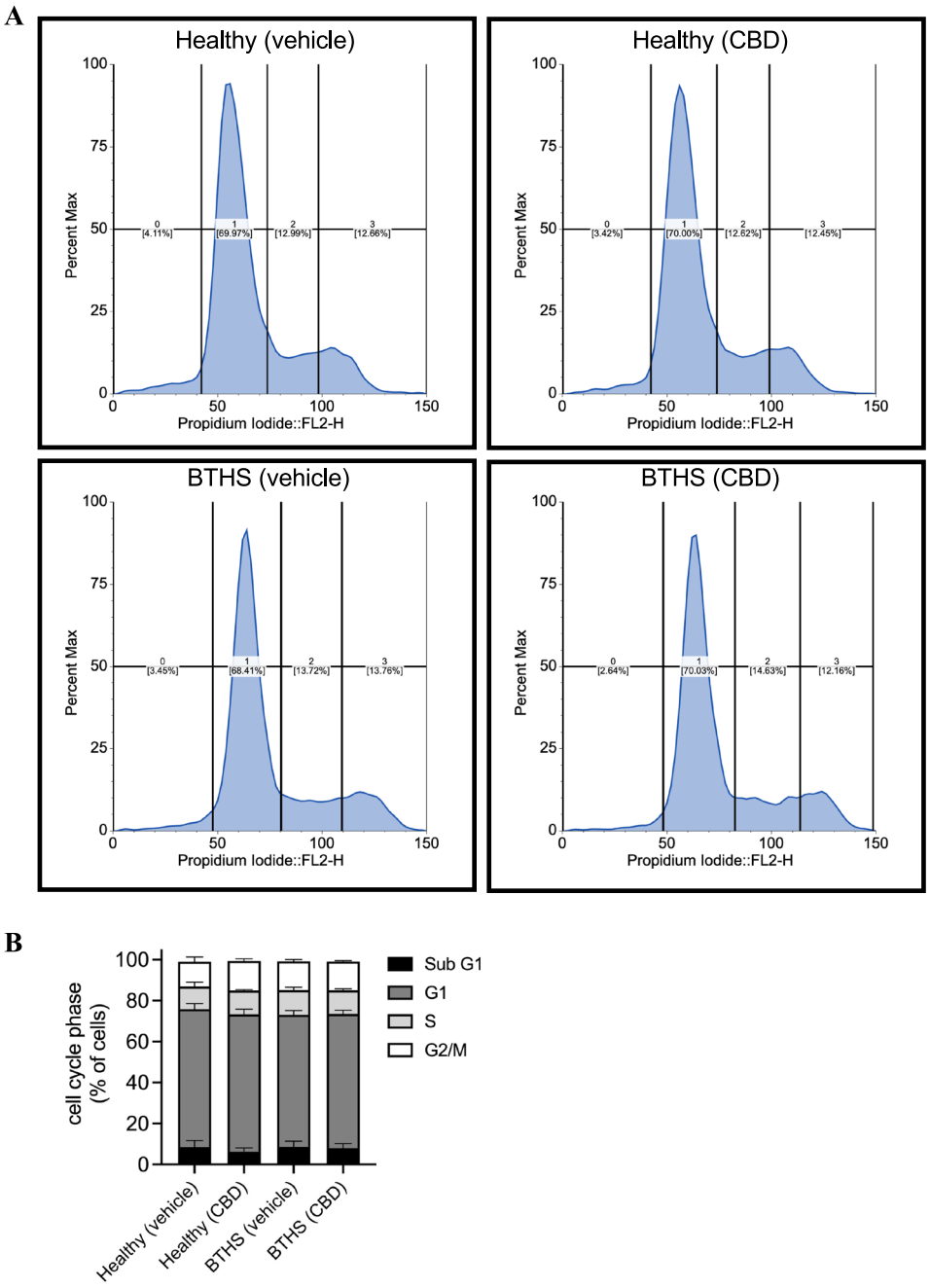

FIGURE 2 | Cell cycle phase proportions of BTHS and Healthy B-lymphoblastoids are similar between groups and unaffected by treatment. Representative flow cytometry cell cycle histograms (A), and means of proportionate cell cycle phase distributions (B) are shown. Data are presented as means ± S.E.M; $n = 5$.

of total SFAs, MUFAs, N-6 PUFAs, or N-3 PUFAs within cardiolipin (Figure 3D–G). CBD treatment also had no effect on the relative proportion of any individual MUFA (Figure 3E) or N-6 PUFA (Figure 3F) within cardiolipin in BTHS B-lymphoblastoids, and had only small effects on other individual fatty acyls. Specifically, in BTHS B-lymphoblastoids, CBD lowered the relative content of 16:0 (Figure 3D) and linolenate (18:3n-3) (Figure 3G), and increased the relative content of 20:3n-3 and 20:4n-3 (Figure 3G). CBD treatment did not alter the relative proportion of any specific fatty acyl species in healthy B-lymphoblastoids.

Examination of the composition of MLCL revealed interesting differences (Figure 3H). The cellular concentration of MLCL SFAs was significantly elevated in vehicle-treated BTHS B-lymphoblastoid cells compared to healthy lines, and this was largely due to higher concentrations of 16:0 and 18:0 (Figure 3H). While MLCL total MUFA concentrations were not significantly elevated, 18:1n-7 was significantly higher in vehicle-treated BTHS B-lymphoblastoids compared to healthy cells (Figure 3H). Notably, treatment with CBD restored MLCL levels of 14:0, 16:0, 18:0, and total SFAs, but not 18:1n-7, to levels comparable to healthy controls (Figure 3H).

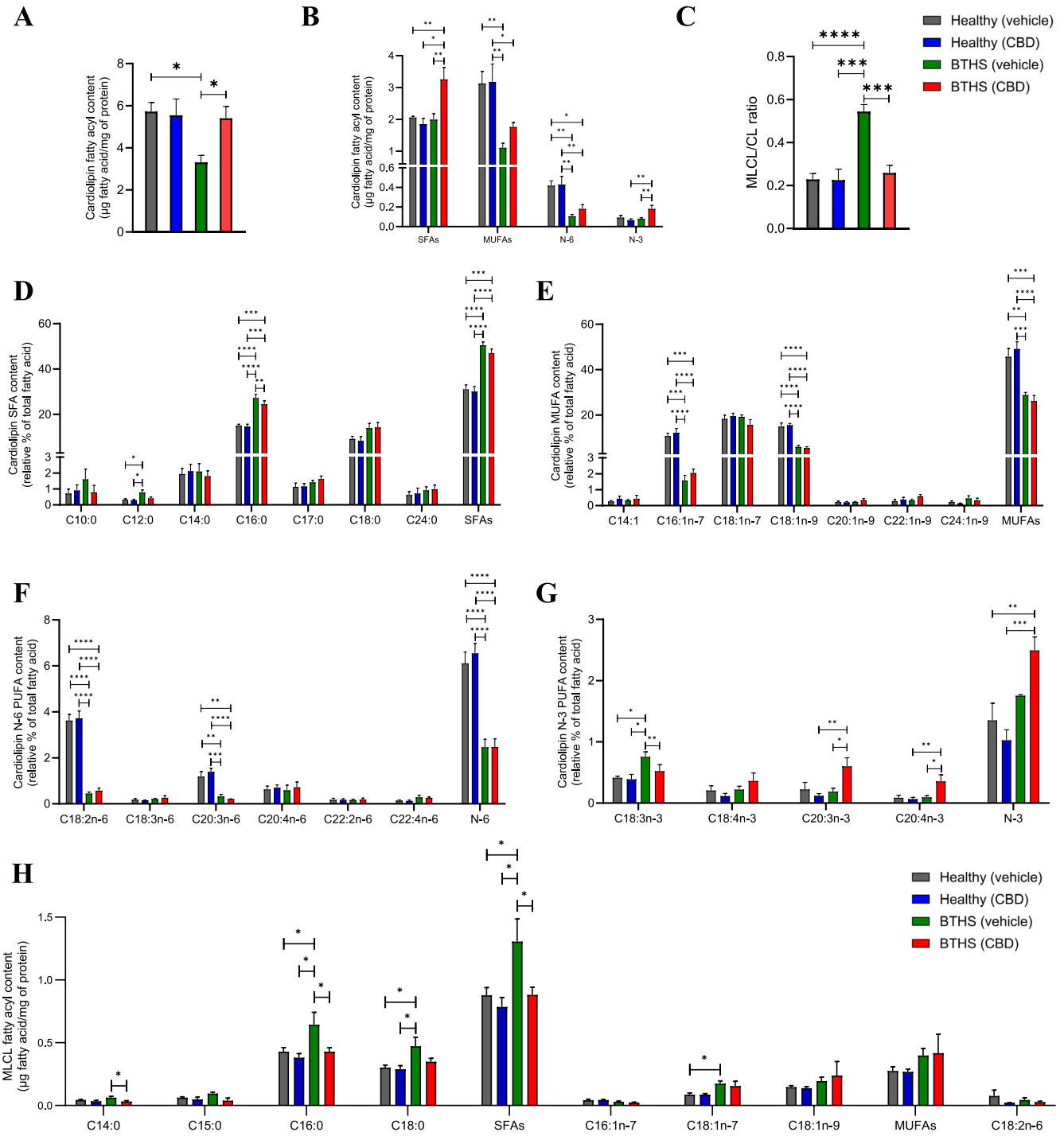

FIGURE 3 | CBD restores total cardiolipin content, and MLCL/CL ratio in BTHS B-lymphoblastoids. Total cardiolipin concentrations (A), cardiolipin fatty acyl concentrations by major categories (B), MLCL/CL ratio (C), relative contents of SFA, MUFA, N-6 PUFA, and N-3 PUFA within cardiolipin (D–G), and the MLCL fatty acyl profile (H) were measured in BTHS and healthy B-lymphoblastoids treated with vehicle or 1 μM CBD. Data are presented as means ± S.E.M; $n = 5$. *$p < 0.05$, **$p < 0.01$, ***$p < 0.001$, ****$p < 0.0001$.

3.4 | CBD Does Not Alter the Expression of Genes Involved in Cardiolipin Biosynthesis, Remodeling, or Deacylation in BTHS B-Lymphoblastoids

The mRNA expression levels of genes involved in cardiolipin biosynthesis (i.e., glycerol-3-phosphate acyltransferase 4 (*GPAT4*), 1-acylglycerol-3-phosphate O-acyltransferase 1 (*AGPAT1*), phosphatidylglycerophosphate synthase (*PGPS*), cardiolipin synthase (*CLS*)), remodeling (i.e., acyl-CoA:lysocardiolipin acyltransferase-1 (*ALCAT1*), and alpha-trifunctional protein (*α-TFP*)), and deacylation (i.e., abhydrolase domain containing 18 (*ABHD18*), patatin-like phospholipase domain-containing protein 8 (*PNPLA8*), phospholipase A2 group VI (*PLA2G6*), and hydroxysteroid 17-beta dehydrogenase 10 (*ABHD10*)) were assessed by qPCR and analyzed relative to *GAPDH* (Figure 4A–J, Table S5A–E). No significant differences were observed between any of the groups.

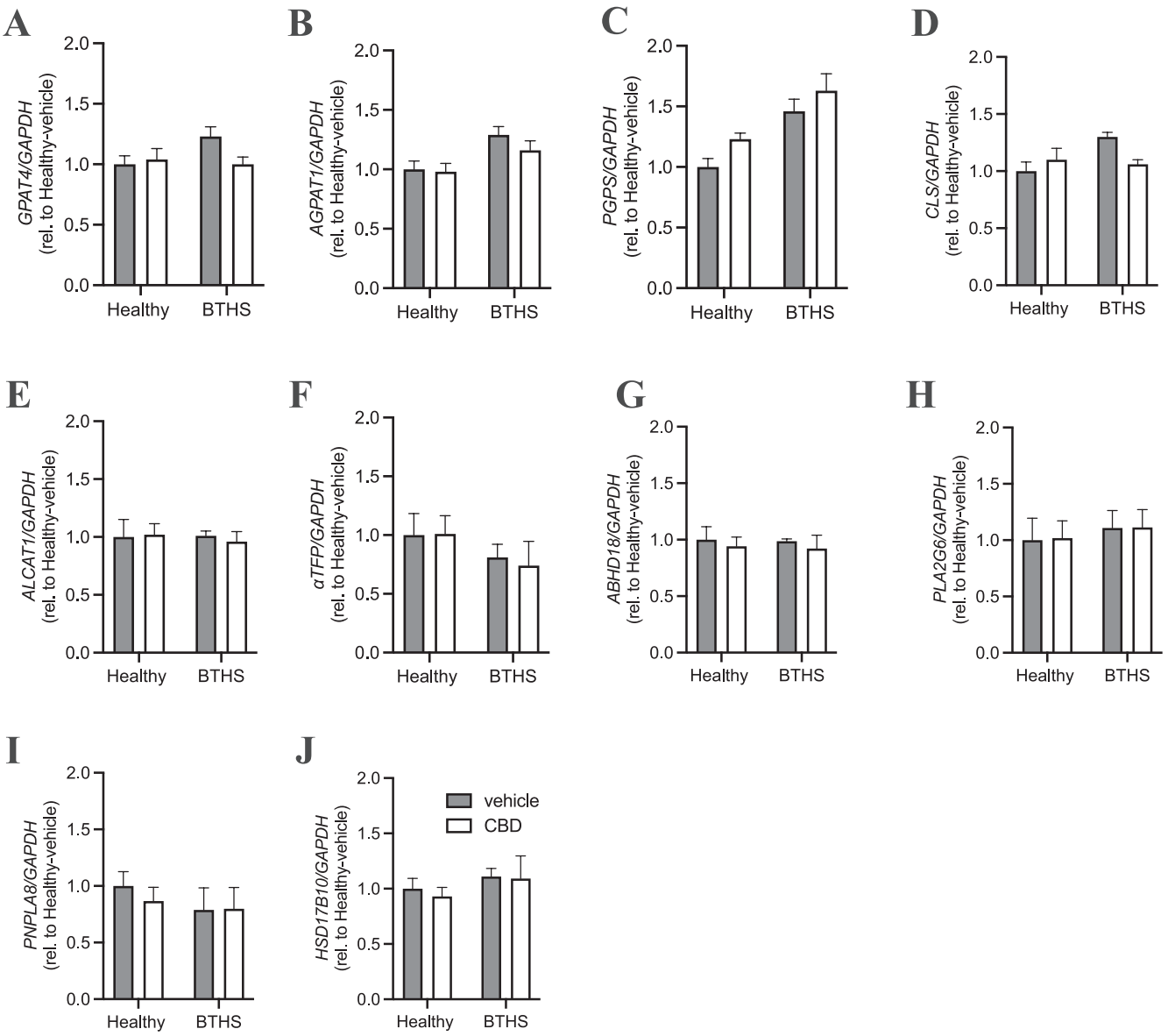

FIGURE 4 | CBD does not alter the expression of genes involved in cardiolipin biosynthesis, remodeling, or deacylation in BTHS B-lymphoblastoids. Expression of genes involved in cardiolipin biosynthesis, remodeling, and deacylation were determined in BTHS and healthy B-lymphoblastoids treated with vehicle or 1 μM CBD, including *GPAT4* (A), *AGPAT1* (B), *PGPS* (C), *CLS* (D), *ALCAT1* (E), *αTFP* (F), *ABHD18* (G), *PLA2G6* (H), *PNPLA8* (I), *and HSD17B10* (J). Data were normalized to *GAPDH* and are presented as fold relative to healthy-vehicle treated means ± S.E.M; $n = 5$.

3.5 | CBD Treatment Does Not Significantly Alter Markers of Mitochondrial Content

Considering the dramatic effect of CBD on the restoration of total cardiolipin levels in BTHS B-lymphoblastoids, we assessed mitochondrial protein markers to determine if there were associated changes that could indicate mitochondrial proliferation. Heat Shock Protein (HSP60) is a mitochondrial chaperone localized primarily to the matrix [40]. Immunodetectable HSP60 was significantly lower in vehicle-treated BTHS compared to healthy B-lymphoblastoids, but levels were not significantly raised by CBD treatment in either group (Figure 5A–C, Figure S1). Peroxisome proliferator-activated receptor γ coactivator 1α (PGC-1α) is a master regulator of mitochondrial biogenesis and cellular energy metabolism [41]. Levels of PGC-1α were similar among all groups and were also unaltered by CBD treatment (Figure 5A,B,D, Figures S2 and S3). Components of the mitochondrial protein import machinery, including translocase of the outer mitochondrial membrane 20 (TOM20) and translocase of the inner mitochondrial membrane 23 (TIM23) were also examined [42, 43]. Levels of both proteins were similar between vehicle-treated BTHS and healthy B-lymphoblastoids (Figure 5A,B,E,F, Figures S9 and S10). CBD treatment did not affect TOM20 levels across both groups but significantly increased TIM23 levels in the BTHS group. MitoTracker Green staining was analyzed using imaging flow cytometry as an additional marker of cellular mitochondrial mass, but no significant differences were detected between any of the groups (Figure 5G,H), strongly suggesting that mitochondrial mass was unaltered by CBD treatment.

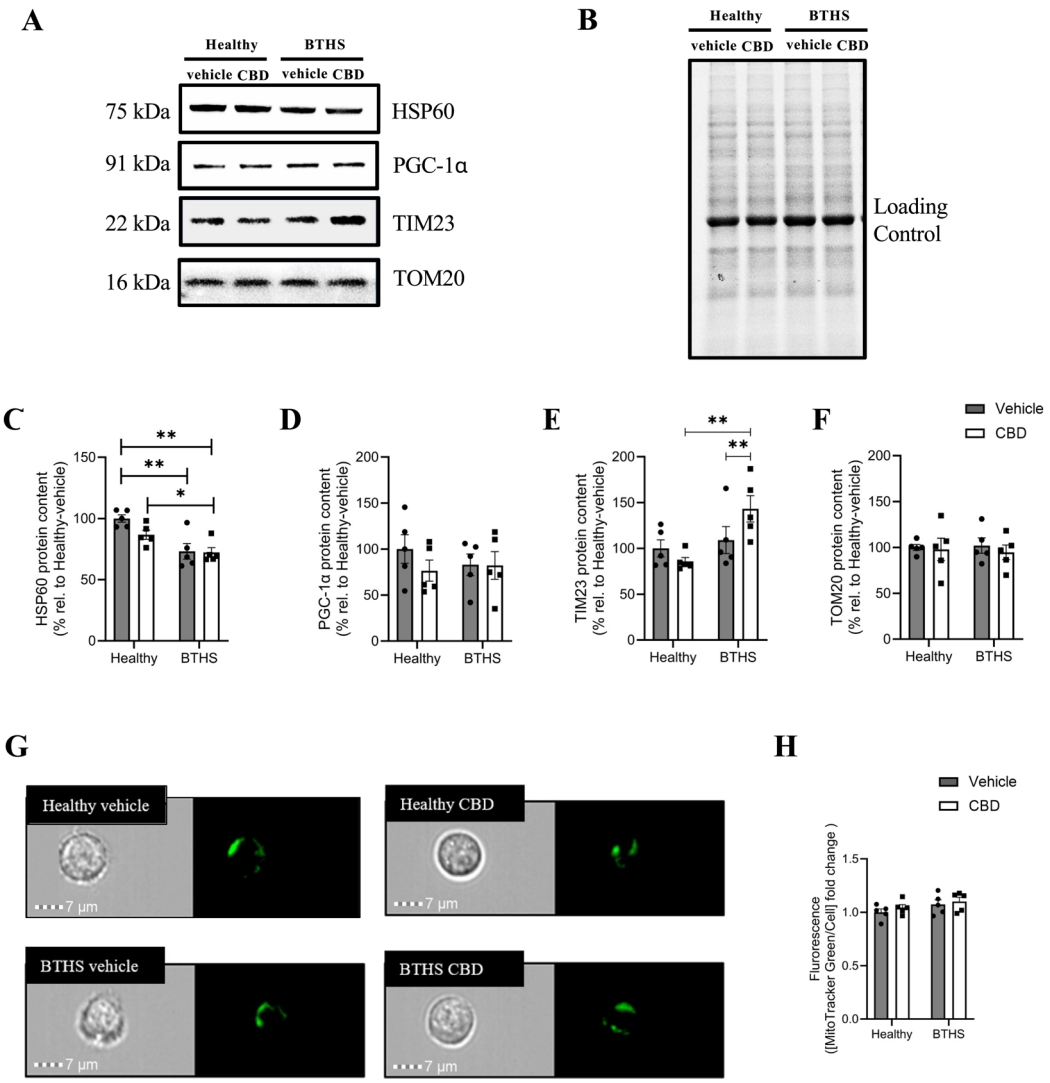

FIGURE 5 | CBD does not change markers of the mitochondrial content of BTHS or healthy B-lymphoblastoids. Representative immunoblots are shown (A) with a representative image of total protein loading (B), with quantitation for band densities, for HSP60 (C), PGC-1α (D), TIM23 (E), and TOM20 (F). Representative brightfield and MitoTracker Green images of vehicle- or CBD-treated healthy and BTHS B-lymphoblastoids are shown (G), along with quantification of MitoTracker Green fluorescence (H). Data are means ± S.E.M; $n = 5$.

3.6 | CBD Increases Maximal Coupled Respiration and MnSOD Content but Does Not Improve Mitochondrial Efficiency in BTHS B-Lymphoblastoids

An increase in cellular cardiolipin concentration, even in the absence of a change in mitochondrial mass, could significantly impact mitochondrial function. We therefore assessed mitochondrial respiration using high-resolution respirometry to measure cellular oxygen consumption following the sequential addition of mitochondrial substrates and ADP. To measure state II respiration mediated by Complex I (CI), pyruvate, malate, and glutamate (PMG) were first introduced. To assess state II respiration mediated by both complex I + II, succinate was sequentially added. While PMG-activated state II respiration was not significantly different between vehicle-treated healthy and BTHS B-lymphoblastoid cells, it was significantly higher in CBD-treated BTHS cells compared to all other groups (Figure 6A). Cellular oxygen consumption activated by PMG + succinate was significantly higher in the vehicle-BTHS group compared to vehicle healthy and higher in the CBD-BTHS group than all other groups (Figure 6A).

Maximal coupled respiration (State III) was evaluated following the addition of 2500 μM ADP, and was not significantly different between vehicle-treated BTHS and healthy B-lymphoblastoids (with or without CBD) (Figure 6A). CBD treatment did not affect the level of State III respiration in healthy cells. However, it significantly increased the maximal respiration of BTHS B-lymphoblastoids.

Mitochondrial coupling efficiency is a measure of the proportion of oxygen consumed by the mitochondria that is used to synthesize adenosine triphosphate (ATP), and it is calculated using the equation, $1 - \left(\frac{\text{State II mediated leak respiration}}{\text{State III ADP – stimulated respiration}}\right)$ [44]. Relative to vehicle-treated healthy controls, vehicle-BTHS B-lymphoblastoids had nearly 40% lower mitochondrial coupling efficiency (Figure 6B).

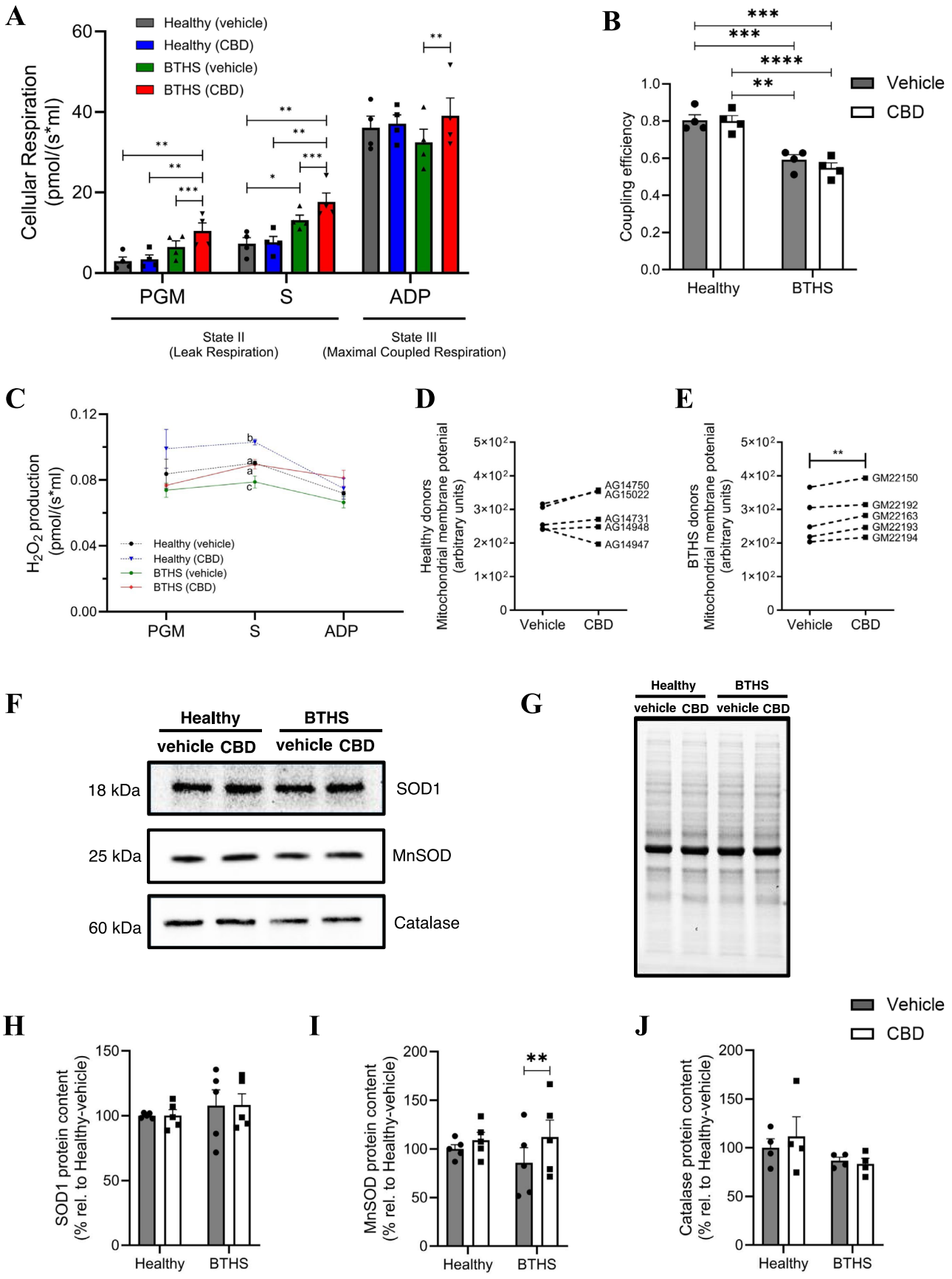

FIGURE 6 | Legend on next page.

FIGURE 6 | CBD increases maximal respiration in BTHS lymphoblastoids but does not improve mitochondrial efficiency. State II (substrate-supported) and State III (ADP-stimulated) respiration rates were measured in digitonin-permeabilized BTHS and healthy B-lymphoblastoids treated with either vehicle control or CBD (A). The mitochondrial coupling efficiency (B) and the effects of CBD treatment on hydrogen peroxide production in BTHS and healthy B-lymphoblastoids are shown in (C). The individual donor response to CBD treatment on the mitochondrial membrane potential of healthy (D) and BTHS (E) B-lymphoblastoids are shown 42 h post treatment. PGM = pyruvate, malate, glutamate, S = succinate, and ADP = adenosine triphosphate. Representative immunoblots, with an image of total protein loading, are shown (F, G), with quantifications for band densities, for SOD1 (H), MnSOD (I), and catalase (J). Data are shown as means ± S.E.M; $n = 4–5$. *$p < 0.05$, **$p < 0.01$, ***$p < 0.001$, ****$p < 0.0001$. [abc]Group means with different letters are significantly different when comparisons are made under the same conditions.

CBD treatment did not significantly alter coupling efficiency in either BTHS or healthy cell lines (Figure 6B).

Hydrogen peroxide (H_2O_2) is a byproduct of mitochondrial respiration, produced when electron leak generates superoxide anions that are rapidly reduced to this more stable species [45]. Electron leak, as evidenced by the rate of H_2O_2 production, was significantly lower in vehicle-treated BTHS compared to healthy cells stimulated with PGM and succinate (Figure 6C). CBD treatment significantly increased the rate of H_2O_2 production in both healthy and BTHS cells, such that levels observed in BTHS cells were restored to healthy-vehicle cell levels, and levels in healthy cells exceeded all groups.

Membrane potential (ΔΨm) measures the voltage difference across the inner mitochondrial membrane generated by the proton gradient established during electron transport [46], and was assessed by flow cytometry following TMRE staining. Although the effect size was relatively modest, all five individual BTHS cell lines showed increases in ΔΨm following CBD treatment, while this parameter was not significantly altered in healthy cells (Figure 6D,E).

To examine the effects of CBD on the antioxidant defense system, immunoblots were performed to determine the relative abundance of several key antioxidant enzymes, including superoxide dismutase 1 (SOD1), manganese superoxide dismutase (MnSOD), and catalase. While no significant differences in the content of SOD1, MnSOD, and catalase were observed between vehicle-treated BTHS and healthy B-lymphoblastoids (Figure 6F–J, Figures S11–S13), treatment with CBD led to a significant increase in MnSOD levels in the BTHS group (Figure 6F,G,I, Figures S12 and S13).

3.7 | CBD Restores SDHA Content and Improves COX I and COX IV Content in BTHS B-Lymphoblastoids

Given the critical role of cardiolipin in ETC stability and function, we performed immunoblotting to quantify the relative levels of various ETC proteins, including the CI protein NADH:ubiquinone oxidoreductase core subunit S1 (NDUFS1), the Complex II (CII) proteins succinate dehydrogenase flavoprotein subunit A (SDHA) and succinate dehydrogenase assembly factor 2 (SDH5), the Complex III (CIII) protein ubiquinol-cytochrome c reductase iron–sulfur subunit (UQCRFS1), the electron carrier Cyt c, and the Complex IV (CIV) proteins cytochrome c oxidase subunit I (COX I) and cytochrome c oxidase subunit IV (COX IV) (Figure 7A–I, Figures S2–S8).

Relative levels of NDUFS1 and UQCRFS1 were similar between vehicle-treated BTHS and healthy B-lymphoblastoids, but SDHA, SDH5, Cyt c, COX I, and COX IV were all lower in BTHS-vehicle cells (Figure 7A–I). Interestingly, treatment with CBD fully restored SDHA to healthy cell levels and partially restored COX I and COX IV levels, but did not ameliorate SDH5 or Cyt c levels. In contrast, immunodetectable ETC proteins in healthy B-lymphoblastoids were largely unaffected by CBD treatment, with the exception that total COX I was 17.8% ± 2.3% lower in healthy cells treated with CBD.

3.8 | CBD Treatment Partially Restored Supercomplex CI/$CIII_2$ Levels but Not CI/$CIII_2$/CIV

B-Lymphoblastoid cells from five BTHS (GM22163, GM22193, GM22194, GM22150, and GM22192) and four healthy (AG14750, AG14948, AG14731, and AG15022) donors were assessed for relative ETC supercomplex levels using BN-PAGE separation, where blots were probed with antibodies specific for CIII (UQCRFS1) and CIV (COX IV), following solubilization of mitochondria with a mild detergent (digitonin) that prevents dissociation of the respiratory supercomplexes (Figure 8A,G, Figure S16) [47]. Immunodetectable CI/$CIII_2$ supercomplex was lower in vehicle-treated BTHS B-lymphoblastoids compared to healthy-vehicle controls, but significantly restored by over 55% on average by treatment with CBD (Figure 8B). Free $CIII_2$ appeared elevated in several of the individual BTHS donor samples, suggesting that it may be destabilized and liberated from higher-order assemblies, although statistical analysis of mean differences did not reach significance due to variation between individual samples (Figure 8C).

Immunodetectable levels of CIV supercomplexes containing COX IV were also significantly lower in vehicle-treated BTHS B-lymphoblastoids compared to healthy-vehicle controls (Figure 8D,E, Figure S16), but were not significantly improved by CBD treatment. Free COX IV-containing CIV levels were significantly lower in vehicle-treated BTHS B-lymphoblastoids compared to vehicle-healthy cells (Figure 8F, Figure S16). However, CBD had no significant effect on CIV or CI/$CIII_2$/IV supercomplex levels, indicating that CBD does not affect CIV stability or supercomplex integration. Total protein loading was assessed by TGX-Stain-free gel imaging (Figure 8G, Figure S16).

4 | Discussion

In this study we utilized B-lymphoblastoid cells derived from age- and sex-matched BTHS and healthy donors in an initial

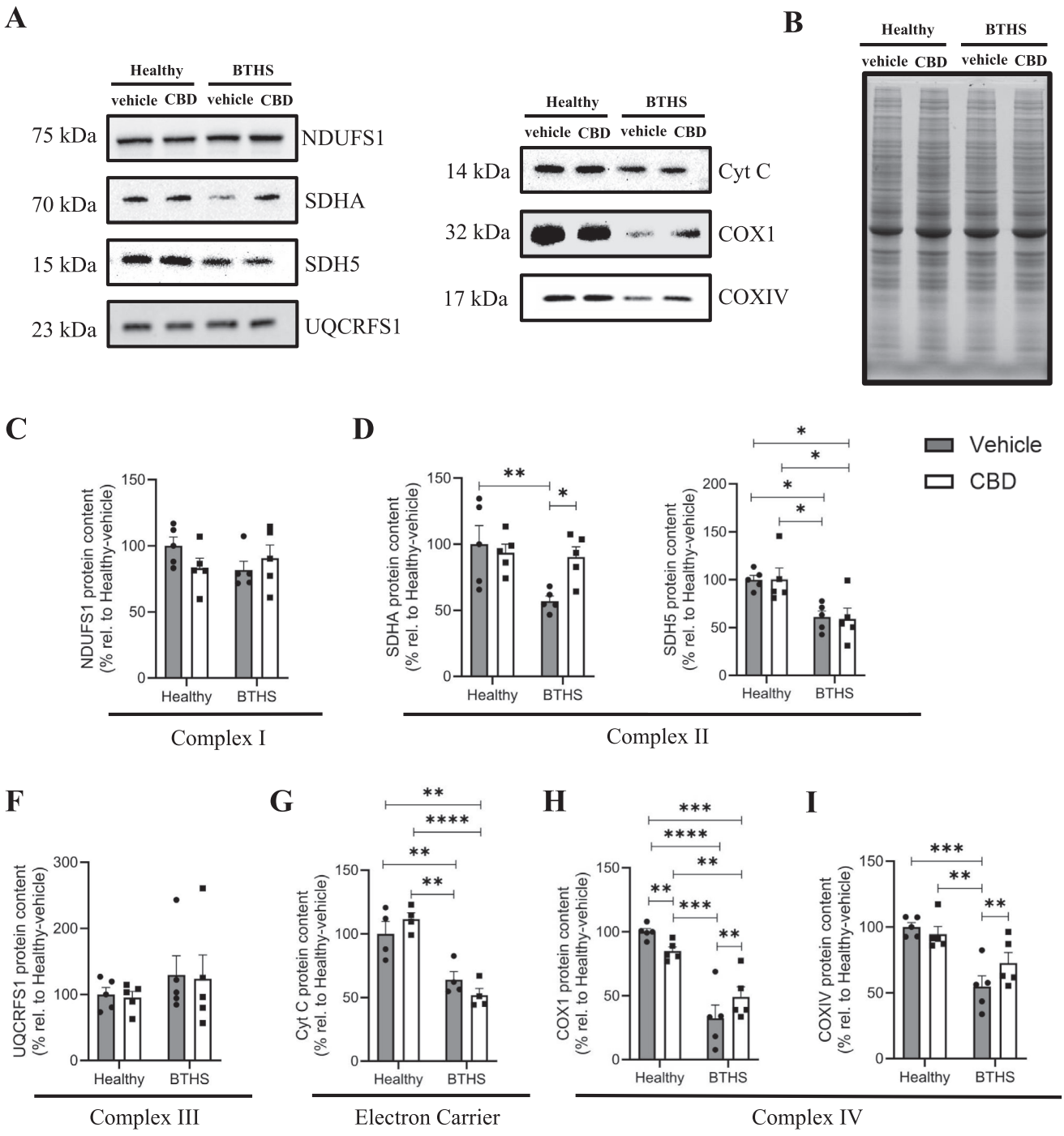

FIGURE 7 | CBD fully restores relative SDHA content and partially restores COXI and COXIV content in BTHS B-lymphoblastoids. Representative immunoblots (A) with images of total protein loading (B) are shown, with quantitation of band densities for NDUFS1 (C), SDHA (D), SDH5 (E), UQCRFS1 (F), Cyt C (G), COXI (H), and COXIV (I). Data are presented as means ± S.E.M, $n = 4–5$. $^{*}p < 0.05$, $^{**}p < 0.01$, $^{***}p < 0.001$, $^{****}p < 0.0001$.

pre-clinical assessment of the therapeutic potential of CBD for the treatment of BTHS lymphopenia, and results were supportive. At present, there is no cure for BTHS, and treatment options largely focus on symptom management [48], including the use of beta-blockers and angiotensin-converting enzyme (ACE) inhibitors for cardiomyopathy, and granulocyte colony-stimulating factor (G-CSF) to reduce infection risk [49]. While advancements have been made in the development of adeno-associated virus (AAV)-mediated gene therapy, this option can be prohibitively expensive and is also not yet available [50–52]. The potential of small molecule therapies therefore remains of clinical interest [53, 54].

Currently, only one small molecule, Elamipretide, has shown therapeutic efficacy. In a Phase 2/3 clinical trial in BTHS patients that was followed by an open-label extension, Elamipretide demonstrated beneficial results in increasing distance traveled during the 6-min walk test and reducing fatigue based on the BTHS Symptom Assessment Scale [54, 55]. Despite these promising results, observed improvements have focused on skeletal

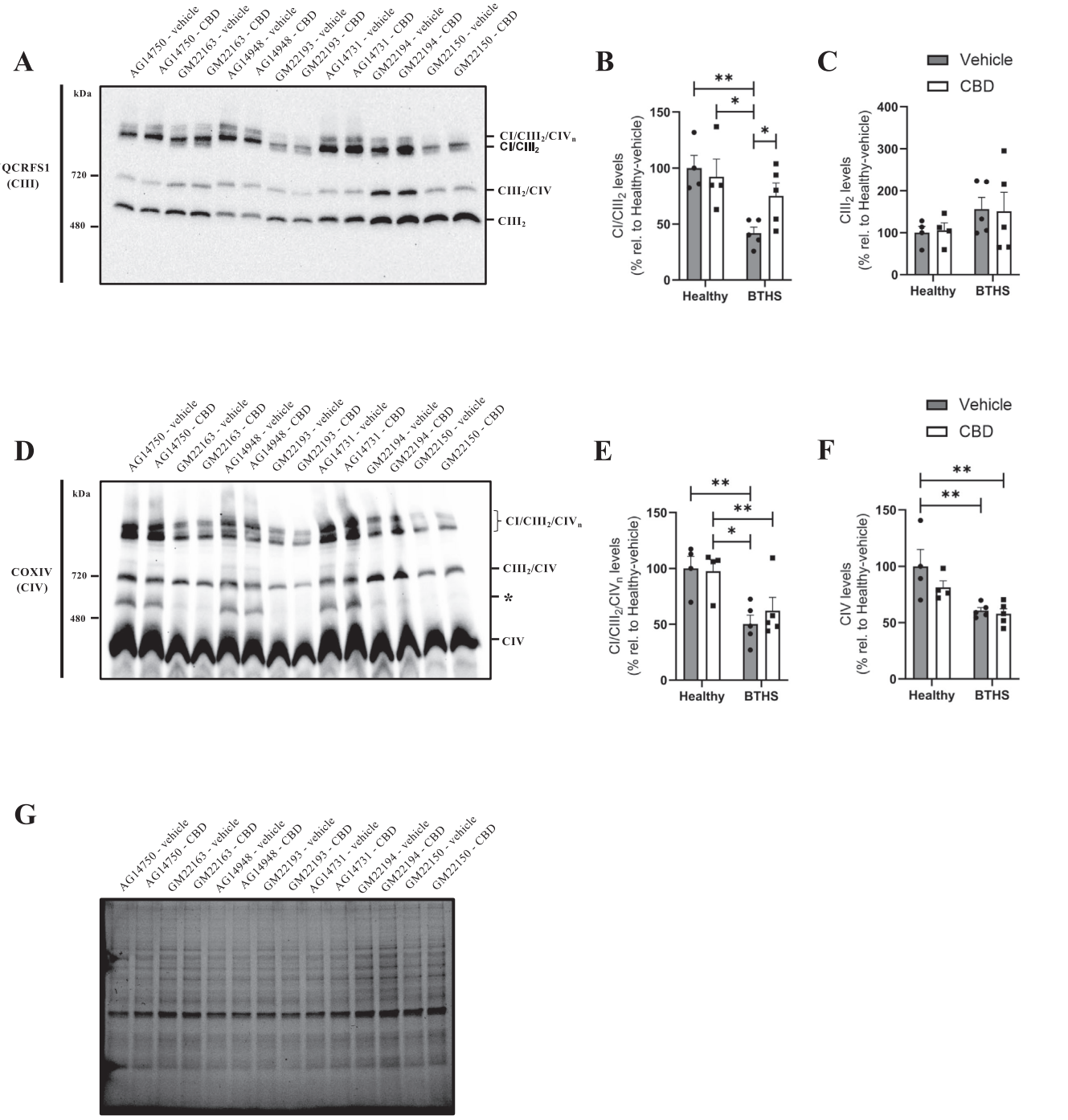

FIGURE 8 | CBD partially restores supercomplex CI/CIII$_2$ levels but has no significant effect on CI/CIII$_2$/CIV. Digitonin solubilized mitochondrial proteins (50 μg) from BTHS and healthy B-lymphoblastoids treated with vehicle or 1 μM CBD were separated by BN-PAGE and probed with antibodies against UQCRFS1 (CIII) (A) and COXIV (CIV) (D). Quantification of band intensities for UQCRFS1 (B, C) and COXIV (E, F) were normalized to total protein per lane from TGX Stain-free SDS-PAGE gels (G). Data are presented as means ± S.E.M; $n = 4–5$. *$p < 0.05$, **$p < 0.01$.

and cardiac functional outcome measures, and effects on immune system dysfunction have not been evaluated. Thus, there is currently a lag in the development of therapeutic strategies targeted at improving the immunological aspects of BTHS, and evidence from this study suggests that CBD may be of value in this regard.

Perhaps the most important finding from this study was the essentially complete rescue of cell growth patterns and numbers over 4 days of culture, which was only partially rescued by the endocannabinoid-like compound OEA in our previous work [11]. Importantly, this result reflected a positive response in each of the five individual BTHS donor lines, while the absence of a response in healthy control cells supports that CBD functions specifically to reverse cellular deficits inherent to BTHS, rather than to effect a non-specific growth promotion. Regardless, the CBD-mediated restoration of BTHS B-lymphoblastoid cell numbers must stem from either an increase in cell proliferation capacity, a decrease in cell death, or a combination of both; therefore, additional investigations were made.

CD8+ T cells isolated from 20-week-old *Tafazzin* knockout mice have been reported to proliferate less efficiently [21]. Furthermore, CBD has been shown to promote cell proliferation in a variety of other cell models through the regulation of cell cycle mediators such as Ki67 and cyclin D1 [56, 57]. Thus, we hypothesized that CBD may help restore growth by facilitating the transition of cells from the quiescent G0 phase into active phases of the cell cycle. Surprisingly, however, no significant differences were detected in the percentage of cells distributed across the G1, S, and G2/M phases between any of the groups tested.

Although this method of testing provides only a snapshot of cell behavior at a single point in time, it strongly suggests that other factors should be considered, including changes in cell death. We examined the proportion of BTHS and healthy B-lymphoblastoids in the sub-G1 population of the cell cycle, which is identified by the presence of DNA fragmentation, a hallmark of late-stage apoptosis [58]. Once again, no significant differences were observed in the percentage of cells within the sub-G1 peak between BTHS and healthy B-lymphoblastoids, suggesting that late-stage apoptosis is not significantly altered in BTHS cells, or by CBD treatment. Notably, however, there are many forms of cell death where DNA fragmentation is not always as distinct, including autophagy [59], pyroptosis [60], ferroptosis [61], and mitoptosis [62], among others [63]. Thus, determining the mechanism of the likely excess cell death in BTHS B-lymphoblastoids, as well as further interactions with CBD as a modulator, will require significant additional study.

Given the critical role of TAFAZZIN in cardiolipin metabolism, our investigation of the effects of CBD in BTHS B-lymphoblastoids focused primarily on mitochondrial alterations linked to the levels and function of this lipid in the inner mitochondrial membrane (IMM). Using TLC-GC, we confirmed the expected significant deficiency in total cardiolipin in BTHS B-lymphoblastoids under vehicle-only conditions, together with the expected shift in the fatty acyl abundance away from a less saturated profile enriched in palmitoleate (16:1n7), oleate (18:1n9), and linoleate (18:2n6) towards one with greater enrichment with palmitate (16:0) and stearate (18:0). In agreement with the magnitude and specificity of rescue of cell growth, treatment of BTHS B-lymphoblastoids with 1 μM CBD resulted in a dramatic and full reversal of the deficiency in total cardiolipin concentration, with no significant effect in healthy control cells. Interestingly, however, this was not associated with a restoration of cardiolipin quality. Following CBD treatment, the only significant change in proportion of a major cardiolipin fatty acyl species in BTHS B-lymphoblastoids was a slight (~2%) reduction in 16:0. Among minor fatty acyls, CBD treatment of BTHS B-lymphoblastoids caused a relative decrease in 18:3n-3 and a relative increase in 20:3n-3, both by only a fraction of a percent.

Taken together, these results suggested that CBD may enhance existing processes of cardiolipin synthesis in BTHS B-lymphoblastoids, or attenuate existing processes of breakdown, without targeting the remodeling of cardiolipin, per se. In particular, investigation of a role for altered ABHD18 activity would be of interest, since a complete normalization of the MLCL/CL ratio and total cardiolipin content was observed in CBD-treated BTHS B-lymphoblastoids, and recent work attributes the rise in MLCL in TAFAZZIN deficiency and loss of cardiolipin total content to enhanced breakdown of cardiolipin by the phospholipase ABHD18 [64, 65]. In these works, the authors identified ABHD18 as a cardiolipin-specific enzyme that interacts with TAFAZZIN to control the relative rate of cardiolipin degradation, with ABHD18 gaining abnormal access to accelerate cardiolipin loss, and promote MLCL generation, in the absence of TAFAZZIN-mediated remodeling [64, 65]. Evaluation of the expression of genes involved in cardiolipin synthesis, remodeling, and breakdown, however, revealed no significant differences, and therefore future mechanistic studies should assess changes in protein levels and activity.

Inadequately remodeled cardiolipin has a bioenergetically unfavorable configuration, and subsequently fails to properly associate with ETC complexes [66]. The normally tight association of cardiolipin with proteins in the IMM is reciprocally both a factor in stabilizing these integral membrane complexes [67] and in the exceptionally long half-life of this lipid, which is protected by these protein-lipid associations [68]. Previous work has found that a loss of ETC protein supercomplex stability is associated with reductions in cardiolipin quantity and quality in BTHS B-lymphoblastoids [12]. We therefore investigated whether CBD treatment affected ETC complex protein levels, supercomplex assembly, and respiration.

Our analyses suggested that the total mitochondrial mass was largely similar between groups. However, mitochondrial function was significantly altered. Although maximal coupled respiration was not statistically lower in BTHS cells compared to healthy controls, CBD raised this measure in BTHS B-lymphoblastoids essentially to control levels, indicating an overall beneficial effect on mitochondrial energetic capacity. This finding is clinically important since mitochondrial output is reduced in BTHS [9, 69, 70]. CBD also increased the $\Delta\Psi m$ in all five treated BTHS B-lymphoblastoid donors, reflecting an increase in the strength of the proton gradient generated by ETC complexes across the inner mitochondrial membrane [46]. Notably, effects of CBD were almost entirely specific to BTHS cells and did not significantly alter measures in healthy B-lymphoblastoids, with the exception of H_2O_2 production, which was increased in both cell lines.

Despite these beneficial changes, CBD treatment also led to an increase in state II-mediated leak respiration in BTHS B-lymphoblastoids. Proton leaks occur when protons bypass ATP synthase and cross the inner mitochondrial membrane without contributing to ATP synthesis [71]. Notably, this leak was able to functionally counteract the CBD-mediated increase in maximal coupled respiration, such that the coupling efficiency remained the same. Another notable effect of CBD treatment is that it significantly increased the rate of H_2O_2 production in BTHS and healthy cells stimulated with PGM and succinate, with levels observed in BTHS cells restored to those observed in healthy controls. This increase in H_2O_2 occurred alongside a CBD-mediated increase in mitochondrial MnSOD in BTHS cells. Given that MnSOD catalyzes the conversion of highly reactive superoxide radicals into the less reactive species H_2O_2, which is subsequently detoxified into water and molecular oxygen by enzymes such as catalase and glutathione peroxidase (GPx) [72],

the observed rise in H_2O_2 is likely a consequence, at least in part, of increased MnSOD levels induced to counteract the increase in superoxide.

While elevated levels of H_2O_2 are implicated in cellular damage, oxidative stress and aging, they are also considered important mediators of normal and even beneficial cellular processes, including autophagy, differentiation, and metabolic adaptation [73]. Given that H_2O_2 is only one of many reactive oxygen species generated by the mitochondria, additional reactive oxygen species such as superoxide and hydroxyl radicals should be examined in future work to provide a more comprehensive understanding of the effects of CBD on oxidative stress in BTHS and healthy B-lymphoblastoids. Regardless, the presence of changes in mitochondrial respiration suggested that additional investigation of ETC complexes and supercomplexes was merited.

Analysis of the relative content of individual respiratory chain subunit proteins indicated significant and specific differences. For example, there was no effect of CBD on relative cellular levels of the CI protein NDUFS1 or CIII protein UQCRFS1, and no difference between healthy and BTHS lines, which was surprising given the well-established role of cardiolipin in maintaining the stability of CI and CIII. However, relative levels of the CII proteins SDHA and SDH5, the electron carrier Cyt c, and the CIV proteins COX I and COX IV, were significantly lower in BTHS B-lymphoblastoid cells, while SHDA was fully restored to control levels, and COX I and COX IV were significantly increased in BTHS lines by CBD treatment.

SDHA is a flavoprotein subunit of CII, which catalyzes the oxidation of succinate to fumarate, transferring electrons to the ubiquinone pool [74]. SDH5 is an assembly factor important for CII stability and function [75]. Although the precise mechanism behind the decrease in SDHA and SDH5 levels in BTHS B-lymphoblastoids remains unclear, previous studies using nanoscale lipid bilayer nanodiscs with varying phospholipid compositions have demonstrated that cardiolipin is necessary for the proper stability and activity of CII [76]. Given that BTHS B-lymphoblastoids are cardiolipin-deficient, it is likely that the observed reductions in SDHA and SDH5 resulted from decreased levels of this IMM lipid, leading to impaired CII assembly and/or stability. The differential restorative effect of CBD on SDHA, in the absence of an effect on SDH5, is interesting and could be related to the role of SDHA as a core protein of the SDH complex, compared to SDH5 that functions as a transient assembly factor [74, 75]. Nevertheless, these results indicate that CBD can have at least a partial beneficial effect on the protein composition of Complex II.

COX I is a catalytic core subunit of Complex IV, responsible for the transfer of electrons from Cyt c to molecular oxygen in cellular respiration, while COX IV plays a regulatory role in stabilizing and optimizing CIV activity [77, 78]. Mechanistically, cardiolipin binds directly to CIV proteins at multiple sites, stabilizing its dimeric structure and optimal electron transfer efficiency [79, 80]. Therefore, the decreased COX I and COX IV levels in BTHS B-lymphoblastoids likely result, at least in part, from cardiolipin deficiency that would lead to improper assembly, and hence increased CIV subunit degradation, while the restoration likely reflects, at least in part, the increased total cardiolipin availability in CBD-treated BTHS cells.

Cyt c functions as a mobile electron carrier between CIII and CIV [81], and its decrease suggests compromised electron transport capacity in BTHS mitochondria. Notably, however, the absence of an effect of CBD on Cyt c levels supports that the therapeutic benefit of this compound in BTHS respiration involves specific ETC components, rather than a general restoration of the system. This leads to an interesting concept that is speculative, but merits further discussion—the potential role of cardiolipin quantity (which was fully restored) versus quality (which changed very little) in the regulation of ETC protein levels.

For example, the present work suggests that specific species of cardiolipin may be required to secure the stability of Cyt c, and the abundance of relative levels of these species may be more important than overall cardiolipin (or MLCL) levels. This may also be the case for COX I and COX IV, which were only modestly increased in CBD-treated cells, in line with the limited improvement of cardiolipin quality observed. Conversely, the full restoration of SDHA levels suggests that this protein may be less selective in its species-specific stabilization by cardiolipin, but sensitive to decreased total levels. Although significant additional work will be required to validate these potential interactions, our findings suggest that further study is warranted.

We next investigated whether improved ETC protein levels translated to an increased assembly of ETC supercomplexes. Supercomplexes are functional, higher-ordered structures consisting of multiple ETC complexes, which promote the efficient transfer of electrons during cellular respiration [82]. In mammalian cells, the most common forms of supercomplexes include the respirasome ($CI/CIII_2/CIV$), $CI/CIII_2$, and $CIII_2/CIV$, with CIII always found as a dimer ($CIII_2$) in these assemblies [82]. A previous study by Mackenize et al. (2006) provided evidence that CIV readily dissociates from supercomplexes and is virtually absent from all higher-order assemblies in BTHS B-lymphoblastoids [12]. Consistent with this, our results revealed significant reductions in supercomplex $CI/CIII_2/CIV$ and free CIV in BTHS cell lines compared to healthy controls. Interestingly, although CBD treatment increased COX I and COX IV subunits in BTHS lymphoblastoids, this increase was not accompanied by any measurable improvement in the higher-order assembly of CIV-containing supercomplexes. In contrast, treatment with CBD partially restored the abundance of the CI/III_2 supercomplex. This work highlights that restoration of cardiolipin content is insufficient to normalize the supercomplexes, and therefore future work should emphasize understanding effects of restoration of cardiolipin quality.

In conclusion, the current work expands our understanding of lymphopenia in BTHS and demonstrates several firsts, including the first evidence that CBD can significantly restore cell population expansion, mitochondrial respiration, cardiolipin total content, and ETC protein levels in cells from patients with BTHS. Further validation in both animal models and humans will be necessary for clinical translation. However, considering the remarkable safety profile of CBD [83], limited side effects, and the beneficial effects of CBD in the current work, further study on

the therapeutic potential of CBD for BTHS is merited. Findings from this work provide a strong basis for future research into the use of CBD as a potential adjuvant treatment for BTHS.

Author Contributions

J.Z.C.: conceptualization, methodology, formal analysis, investigation, data curation, writing – original draft, writing – review and editing; A.N.B.: conceptualization, methodology, formal analysis, investigation, data curation, writing – original draft, writing – review and editing; M.R.L.: methodology, formal analysis, investigation, data curation, writing – review and editing; F.A.R.: methodology, formal analysis, investigation, data curation, writing – review and editing; M.V.T.: methodology, formal analysis, investigation, data curation, writing – review and editing. M.Q.G.: methodology, formal analysis, investigation, data curation, writing – review and editing; M.M.: investigation, writing – review and editing; A.D.C.: investigation, writing – review and editing; K.D.S.: methodology, data curation, writing – original draft, writing – review and editing, Supervision, funding acquisition; J.Q.: funding acquisition, supervision, writing – review and editing. R.E.D.: conceptualization, methodology, formal analysis, data curation, writing – original draft, writing – review and editing, supervision, funding acquisition.

Funding

This work was supported by Discovery Grants and a Discovery Accelerator Supplement Award from the Natural Sciences and Engineering Research Council of Canada (NSERC) #RGPAS-2019-00008, #RGPIN-2019-05642, #RGPIN-2012-418 213 and RGPAS-2019-00008, #RTI-2022-00006, #NSERC-CGS-M, #NSERC-CGS-D, #RGPIN-2024-04421, #NSERC-USRA by Idea grants (2015 and 2019) from the Barth Syndrome Foundation, the Barth Syndrome Foundation of Canada IdeaGrant2015, IdeaGrant2019, and the Barth Syndrome Foundation UK, as well as the Canada Foundation for Innovation—Leader's Opportunity Fund and Government of Ontario—Ontario Research Fund (Project No. 30259), ORF#30259, ER16-12-162, and Government of Ontario Early Researcher Award (ERA)—to R.E.D. Funding was provided to J.Q. by NSERC Discovery Grant #RGPIN-2025-04908. J.Z.C., M.V.T., and F.A.R. were supported by Canada Graduate Research Scholarships-Doctoral (CGS-D) from NSERC, and A.N.B. was supported by a Canada Graduate Research Scholarship-Masters (CGS-M) from NSERC. M.Q.G. and M.M. were supported by NSERC Undergraduate Student Research Awards.

Conflicts of Interest

K.D.S. is currently on the Board of Directors of the International Society for the Study of Fatty Acids and Lipids. R.E.D. hold shares in Akseera Pharma Corp. that is engaged in research and commercialization activities related to the therapeutic potential of cannabinoids (< 5% of total issued shares) but is not involved in the direction or operations of the company. Akseera Pharma Corp. did not participate in the funding or conduct of this work. R.E.D. is a co-inventor on international applications under the Patent Cooperation Treaty related to the therapeutic potential of cannabinoids entitled "Interaction of Sars-Cov-2 proteins with molecular and cellular mechanisms of host cells and formulations to treat COVID-19" (WO 2021/199078 A2 and WO 2022/018754 A1), "Augmentation of anti-viral and anti-cancer treatments by combinations of Poly (I:C) and Cannabidiol" (WO 2023/187842 A3) and "A method for use of cannabidiol in the prevention and treatment of interferon-responsive conditions" (WO 2023/195029 A2).

Data Availability Statement

The data that support the findings of this study are available in the Materials and Methods, Results, and/or Supporting Information of this article.

References

1. J. Dudek and C. Maack, "Barth Syndrome Cardiomyopathy," *Cardiovascular Research* 113 (2017): 399–410.

2. P. C. Miller, M. Ren, M. Schlame, M. J. Toth, and C. K. L. Phoon, "A Bayesian Analysis to Determine the Prevalence of Barth Syndrome in the Pediatric Population," *Journal of Pediatrics* 217 (2020): 139–144.

3. *Human Tafazzin Gene Variants database.* Barth Syndrome Foundation. (n.d.), https://www.barthsyndrome.org/research/tafazzindatabase.html.

4. S. Zhu, Z. Chen, M. Zhu, et al., "Cardiolipin Remodeling Defects Impair Mitochondrial Architecture and Function in a Murine Model of Barth Syndrome Cardiomyopathy," *Circulation. Heart Failure* 14 (2021): e008289.

5. G. A. Shilovsky, O. A. Zverkov, A. V. Seliverstov, et al., "New C-Terminal Conserved Regions of Tafazzin, a Catalyst of Cardiolipin Remodeling," *Oxidative Medicine and Cellular Longevity* 2019 (2019): 2901057.

6. Y. Xu, R. I. Kelley, T. J. Blanck, and M. Schlame, "Remodeling of Cardiolipin by Phospholipid Transacylation," *Journal of Biological Chemistry* 278 (2003): 51380–51385.

7. F. Valianpour, V. Mitsakos, D. Schlemmer, et al., "Monolysocardiolipins Accumulate in Barth Syndrome but Do Not Lead to Enhanced Apoptosis," *Journal of Lipid Research* 46 (2005): 1182–1195.

8. D. Acehan, F. Vaz, R. H. Houtkooper, et al., "Cardiac and Skeletal Muscle Defects in a Mouse Model of Human Barth Syndrome," *Journal of Biological Chemistry* 286 (2011): 899–908.

9. F. Gonzalvez, M. D'Aurelio, M. Boutant, et al., "Barth Syndrome: Cellular Compensation of Mitochondrial Dysfunction and Apoptosis Inhibition due to Changes in Cardiolipin Remodeling Linked to Tafazzin (TAZ) Gene Mutation," *Biochimica et Biophysica Acta* 1832 (2013): 1194–1206.

10. D. Acehan, Y. Xu, D. L. Stokes, and M. Schlame, "Comparison of Lymphoblast Mitochondria From Normal Subjects and Patients With Barth Syndrome Using Electron Microscopic Tomography," *Laboratory Investigation* 87 (2007): 40–48.

11. J. Z. Chan, M. F. Fernandes, K. E. Steckel, et al., "N-Oleoylethanolamide Treatment of Lymphoblasts Deficient in Tafazzin Improves Cell Growth and Mitochondrial Morphology and Dynamics," *Scientific Reports* 12 (2022): 9466.

12. M. McKenzie, M. Lazarou, D. R. Thorburn, and M. T. Ryan, "Mitochondrial Respiratory Chain Supercomplexes Are Destabilized in Barth Syndrome Patients," *Journal of Molecular Biology* 361 (2006): 462–469.

13. S. C. Clarke, A. Bowron, I. L. Gonzalez, et al., "Barth Syndrome," *Orphanet Journal of Rare Diseases* 8 (2013): 23.

14. J. Pang, Y. Bao, K. Mitchell-Silbaugh, J. Veevers, and X. Fang, "Barth Syndrome Cardiomyopathy: An Update," *Genes* 13 (2022): 656.

15. V. Raja, C. A. Reynolds, and M. L. Greenberg, "Barth Syndrome: A Life-Threatening Disorder Caused by Abnormal Cardiolipin Remodeling," *Journal of Rare Diseases Research & Treatment* 2 (2017): 58–62.

16. V. Makaryan, W. Kulik, F. M. Vaz, et al., "The Cellular and Molecular Mechanisms for Neutropenia in Barth Syndrome," *European Journal of Haematology* 88 (2012): 195–209.

17. C. G. Steward, S. J. Groves, C. T. Taylor, et al., "Neutropenia in Barth Syndrome: Characteristics, Risks, and Management," *Current Opinion in Hematology* 26 (2019): 6–15.

18. B. J. van Raam and T. W. Kuijpers, "Mitochondrial Defects Lie at the Basis of Neutropenia in Barth Syndrome," *Current Opinion in Hematology* 16 (2009): 14–19.

19. J. Finsterer and M. Frank, "Haematological Features in Barth Syndrome," *Current Opinion in Hematology* 20 (2013): 36–40.

20. J. Sohn, J. Milosevic, T. Brouse, et al., "A New Murine Model of Barth Syndrome Neutropenia Links TAFAZZIN Deficiency to Increased ER Stress-Induced Apoptosis," *Blood Advances* 6 (2022): 2557–2577.

21. M. Corrado, J. Edwards-Hicks, M. Villa, et al., "Dynamic Cardiolipin Synthesis Is Required for CD8(+) T Cell Immunity," *Cell Metabolism* 32 (2020): 981–995.

22. H. M. Zegallai, K. Duan, and G. M. Hatch, "Reduction in mRNA Expression of the Neutrophil Chemoattract Factor CXCL1 in *Pseudomonas aeruginosa* Treated Barth Syndrome B Lymphoblasts," *Biology-Basel* 12 (2023): 730.

23. E. A. Kudlaty, N. Agnihotri, and A. Khojah, "Hypogammaglobulinaemia and B Cell Lymphopaenia in Barth Syndrome," *BMJ Case Reports* 15 (2022): e249254.

24. M. J. Nielsen, G. Petersen, A. Astrup, and H. S. Hansen, "Food Intake Is Inhibited by Oral Oleoylethanolamide," *Journal of Lipid Research* 45 (2004): 1027–1029.

25. I. Ujvary and L. Hanus, "Human Metabolites of Cannabidiol: A Review on Their Formation, Biological Activity, and Relevance in Therapy," *Cannabis and Cannabinoid Research* 1 (2016): 90–101.

26. R. Adams, M. Hunt, and J. H. Clark, "Structure of Cannabidiol, a Product Isolated From the Marihuana Extract of Minnesota Wild Hemp," *Journal of the American Chemical Society* 62 (1940): 196–200.

27. J. Z. Chan and R. E. Duncan, "Regulatory Effects of Cannabidiol on Mitochondrial Functions: A Review," *Cells* 10 (2021): 1251.

28. J. M. Fuentes and P. Morcillo, "The Role of Cardiolipin in Mitochondrial Function and Neurodegenerative Diseases," *Cells* 13 (2024): 609.

29. Y. Shi, "Emerging Roles of Cardiolipin Remodeling in Mitochondrial Dysfunction Associated With Diabetes, Obesity, and Cardiovascular Diseases," *Journal of Biomedical Research* 24 (2010): 6–15.

30. K. Boonstra, D. Bloemberg, and J. Quadrilatero, "Caspase-2 Is Required for Skeletal Muscle Differentiation and Myogenesis," *Biochimica et Biophysica Acta* 1865 (2018): 95–104.

31. E. G. Bligh and W. J. Dyer, "A Rapid Method of Total Lipid Extraction and Purification," *Canadian Journal of Biochemistry and Physiology* 37 (1959): 911–917.

32. A. Hashemi, M. R. Liu, J. Z. Chan, et al., "Plaat1 Deficiency Reduces Cardiac Cardiolipin Content and Impairs Exercise Tolerance," *Journal of Lipid Research* 66 (2025): 100822.

33. W. R. Morrison and L. M. Smith, "Preparation of Fatty Acid Methyl Esters and Dimethylacetals From Lipids With Boron Fluoride–Methanol," *Journal of Lipid Research* 5 (1964): 600–608.

34. M. V. Tomczewski, J. Z. Chan, D. M. Al-Majmaie, et al., "Phenotypic Characterization of Female Carrier Mice Heterozygous for Tafazzin Deletion," *Biology-Basel* 12 (2023): 1238.

35. L. García-Prat, M. Martínez-Vicente, and P. Muñoz-Cánoves, "Methods for Mitochondria and Mitophagy Flux Analyses in Stem Cells of Resting and Regenerating Skeletal Muscle," *Methods in Molecular Biology (Clifton, N.J.)* 1460 (2016): 223–240.

36. L. Garcia-Prat, M. Martinez-Vicente, E. Perdiguero, et al., "Autophagy Maintains Stemness by Preventing Senescence," *Nature* 529 (2016): 37–42.

37. J. Z. Chan, M. F. Fernandes, A. Hashemi, et al., "Age-Associated Increase in Anxiety-Like Behavior in Lpaatδ/Agpat4 Knockout Mice," *Current Research in Behavioral Sciences* 2 (2021): 100042.

38. M. M. M. Abou-Hashem, D. M. Abo-Elmatty, N. M. Mesbah, and A. M. Abd El-Mawgoud, "Induction of Sub-G(0) Arrest and Apoptosis by Seed Extract of Moringa Peregrina (Forssk.) Fiori in Cervical and Prostate Cancer Cell Lines," *Journal of Integrative Medicine* 17 (2019): 410–422.

39. E. D. Israels and L. G. Israels, "The Cell Cycle," *Oncologist* 5 (2000): 510–513.

40. M. Y. Cheng, F. U. Hartl, and A. L. Horwich, "The Mitochondrial Chaperonin hsp60 Is Required for Its Own Assembly," *Nature* 348 (1990): 455–458.

41. J. F. Halling and H. Pilegaard, "PGC-1alpha-Mediated Regulation of Mitochondrial Function and Physiological Implications," *Applied Physiology, Nutrition, and Metabolism = Physiologie Appliquee, Nutrition et Metabolisme* 45 (2020): 927–936.

42. Y. Araiso, K. Imai, and T. Endo, "Role of the TOM Complex in Protein Import Into Mitochondria: Structural Views," *Annual Review of Biochemistry* 91 (2022): 679–703.

43. K. Demishtein-Zohary and A. Azem, "The TIM23 Mitochondrial Protein Import Complex: Function and Dysfunction," *Cell and Tissue Research* 367 (2017): 33–41.

44. S. Djafarzadeh and S. M. Jakob, "High-Resolution Respirometry to Assess Mitochondrial Function in Permeabilized and Intact Cells," *Journal of Visualized Experiments: JoVE* 8 (2017): 54985.

45. T. Sakamoto and H. Imai, "Hydrogen Peroxide Produced by Superoxide Dismutase SOD-2 Activates Sperm in *Caenorhabditis elegans*," *Journal of Biological Chemistry* 292 (2017): 14804–14813.

46. L. D. Zorova, V. A. Popkov, E. Y. Plotnikov, et al., "Mitochondrial Membrane Potential," *Analytical Biochemistry* 552 (2018): 50–59.

47. H. Schägger and K. Pfeiffer, "Supercomplexes in the Respiratory Chains of Yeast and Mammalian Mitochondria," *EMBO Journal* 19 (2000): 1777–1783.

48. S. Reynolds, "Successful Management of Barth Syndrome: A Systematic Review Highlighting the Importance of a Flexible and Multidisciplinary Approach," *Journal of Multidisciplinary Healthcare* 8 (2015): 345–358.

49. V. Raja, C. Reynolds, and M. L. Greenberg, "A Life-Threatening Disorder Caused by Abnormal Cardiolipin Remodeling," *Journal of Rare Disease Research & Treatment* 2 (2017): 58–62.

50. S. Suzuki-Hatano, M. Saha, S. A. Rizzo, et al., "AAV-Mediated TAZ Gene Replacement Restores Mitochondrial and Cardioskeletal Function in Barth Syndrome," *Human Gene Therapy* 30 (2019): 139–154.

51. S. Wang, Y. Li, Y. Xu, et al., "AAV Gene Therapy Prevents and Reverses Heart Failure in a Murine Knockout Model of Barth Syndrome," *Circulation Research* 126 (2020): 1024–1039.

52. C. H. Wong, D. Li, N. Wang, J. Gruber, A. W. Lo, and R. M. Conti, "The Estimated Annual Financial Impact of Gene Therapy in the United States," *Gene Therapy* 30 (2023): 761–773.

53. Y. Huang, C. Powers, V. Moore, et al., "The PPAR Pan-Agonist Bezafibrate Ameliorates Cardiomyopathy in a Mouse Model of Barth Syndrome," *Orphanet Journal of Rare Diseases* 12 (2017): 49.

54. H. N. Sabbah, "Elamipretide for Barth Syndrome Cardiomyopathy: Gradual Rebuilding of a Failed Power Grid," *Heart Failure Reviews* 27 (2022): 1911–1923.

55. W. Reid Thompson, B. Hornby, R. Manuel, et al., "A Phase 2/3 Randomized Clinical Trial Followed by an Open-Label Extension to Evaluate the Effectiveness of Elamipretide in Barth Syndrome, a Genetic Disorder of Mitochondrial Cardiolipin Metabolism," *Genetics in Medicine* 23 (2021): 471–478.

56. P. Montreekachon, N. Chaichana, A. Makeudom, V. Kerdvongbundit, W. Krisanaprakornkit, and S. Krisanaprakornkit, "Proliferative Effect of Cannabidiol in Human Gingival Fibroblasts via the Mitogen-Activated Extracellular Signal-Regulated Kinase (MEK) 1/2," *Journal of Periodontal Research* 58 (2023): 1223–1234.

57. M. Gerasymchuk, G. I. Robinson, A. Groves, et al., "Phytocannabinoids Stimulate Rejuvenation and Prevent Cellular Senescence in Human Dermal Fibroblasts," *Cells* 11 (2022): 3939.

58. L. F. He and J. G. Chen, "DNA Damage, Apoptosis and Cell Cycle Changes Induced by Fluoride in Rat Oral Mucosal Cells and Hepatocytes," *World Journal of Gastroenterology* 12 (2006): 1144–1148.

59. S. Liu, S. Yao, H. Yang, S. Liu, and Y. Wang, "Autophagy: Regulator of Cell Death," *Cell Death & Disease* 14 (2023): 648.

60. P. Yu, X. Zhang, N. Liu, L. Tang, C. Peng, and X. Chen, "Pyroptosis: Mechanisms and Diseases," *Signal Transduction and Targeted Therapy* 6 (2021): 128.

61. J. Li, F. Cao, H. L. Yin, et al., "Ferroptosis: Past, Present and Future," *Cell Death & Disease* 11 (2020): 88.

62. J. R. Jangamreddy and M. J. Los, "Mitoptosis, a Novel Mitochondrial Death Mechanism Leading Predominantly to Activation of Autophagy," *Hepatitis Monthly* 12 (2012): e6159.

63. G. Yan, M. Elbadawi, and T. Efferth, "Multiple Cell Death Modalities and Their Key Features (Review)," *World Academy of Sciences Journal* 2 (2020): 39–48.

64. S. N. Masud, A. Srivastava, P. Mero, et al., "Genetic Suppression Features ABHD18 as a Barth Syndrome Therapeutic Target," *Nature* 645 (2025): 1029–1038.

65. M. Ren, S. Chen, M. L. Greenberg, and M. Schlame, "ABHD18 Degrades Cardiolipin by Stepwise Hydrolysis of Fatty Acids," *Journal of Biological Chemistry* 301 (2025): 110237.

66. E. R. Pennington, K. Funai, D. A. Brown, and S. R. Shaikh, "The Role of Cardiolipin Concentration and Acyl Chain Composition on Mitochondrial Inner Membrane Molecular Organization and Function," *Biochimica et Biophysica Acta, Molecular and Cell Biology of Lipids* 1864 (2019): 1039–1052.

67. A. Musatov and E. Sedlak, "Role of Cardiolipin in Stability of Integral Membrane Proteins," *Biochimie* 142 (2017): 102–111.

68. Y. Xu, C. K. Phoon, B. Berno, et al., "Loss of Protein Association Causes Cardiolipin Degradation in Barth Syndrome," *Nature Chemical Biology* 12 (2016): 641–647.

69. M. A. Kiebish, K. Yang, X. Liu, et al., "Dysfunctional Cardiac Mitochondrial Bioenergetic, Lipidomic, and Signaling in a Murine Model of Barth Syndrome," *Journal of Lipid Research* 54 (2013): 1312–1325.

70. L. Ma, F. M. Vaz, Z. Gu, R. J. Wanders, and M. L. Greenberg, "The Human TAZ Gene Complements Mitochondrial Dysfunction in the Yeast taz1Delta Mutant. Implications for Barth Syndrome," *Journal of Biological Chemistry* 279 (2004): 44394–44399.

71. J. Cheng, G. Nanayakkara, Y. Shao, et al., "Mitochondrial Proton Leak Plays a Critical Role in Pathogenesis of Cardiovascular Diseases," *Advances in Experimental Medicine and Biology* 982 (2017): 359–370.

72. C. J. Weydert and J. J. Cullen, "Measurement of Superoxide Dismutase, Catalase and Glutathione Peroxidase in Cultured Cells and Tissue," *Nature Protocols* 5 (2010): 51–66.

73. L. A. Sena and N. S. Chandel, "Physiological Roles of Mitochondrial Reactive Oxygen Species," *Molecular Cell* 48 (2012): 158–167.

74. E. Goetzman, Z. Gong, B. Zhang, and R. Muzumdar, "Complex II Biology in Aging, Health, and Disease," *Antioxidants* 12 (2023): 1477.

75. L. Oudijk, J. Gaal, and R. R. de Krijger, "The Role of Immunohistochemistry and Molecular Analysis of Succinate Dehydrogenase in the Diagnosis of Endocrine and Non-Endocrine Tumors and Related Syndromes," *Endocrine Pathology* 30 (2019): 64–73.

76. C. T. Schwall, V. L. Greenwood, and N. N. Alder, "The Stability and Activity of Respiratory Complex II Is Cardiolipin-Dependent," *Biochimica et Biophysica Acta* 1817 (2012): 1588–1596.

77. M. Brischigliaro and M. Zeviani, "Cytochrome c Oxidase Deficiency," *Biochimica et Biophysica Acta - Bioenergetics* 1862 (2021): 148335.

78. Y. Li, J. S. Park, J. H. Deng, and Y. Bai, "Cytochrome c Oxidase Subunit IV Is Essential for Assembly and Respiratory Function of the Enzyme Complex," *Journal of Bioenergetics and Biomembranes* 38 (2006): 283–291.

79. G. Paradies, V. Paradies, V. De Benedictis, F. M. Ruggiero, and G. Petrosillo, "Functional Role of Cardiolipin in Mitochondrial Bioenergetics," *Biochimica et Biophysica Acta* 1837 (2014): 408–417.

80. A. Musatov and N. C. Robinson, "Bound Cardiolipin Is Essential for Cytochrome c Oxidase Proton Translocation," *Biochimie* 105 (2014): 159–164.

81. M. Huttemann, P. Pecina, M. Rainbolt, et al., "The Multiple Functions of Cytochrome c and Their Regulation in Life and Death Decisions of the Mammalian Cell: From Respiration to Apoptosis," *Mitochondrion* 11 (2011): 369–381.

82. S. Guan, L. Zhao, and R. Peng, "Mitochondrial Respiratory Chain Supercomplexes: From Structure to Function," *International Journal of Molecular Sciences* 23 (2022): 13880.

83. K. Iffland and F. Grotenhermen, "An Update on Safety and Side Effects of Cannabidiol: A Review of Clinical Data and Relevant Animal Studies," *Cannabis and Cannabinoid Research* 2 (2017): 139–154.

Supporting Information

Additional supporting information can be found online in the Supporting Information section. **Data S1:** Supporting Information.